

1 **Ground-level gaseous pollutants (NO<sub>2</sub>, SO<sub>2</sub>, and CO) in**  
2 **China: daily seamless mapping and spatiotemporal**  
3 **variations**

4  
5 Jing Wei<sup>1\*</sup>, Zhanqing Li<sup>1\*</sup>, Jun Wang<sup>2</sup>, Can Li<sup>1</sup>, Pawan Gupta<sup>3,4</sup>, Maureen Cribb<sup>1</sup>  
6

7 1. Department of Atmospheric and Oceanic Science, Earth System Science Interdisciplinary  
8 Center, University of Maryland, College Park, MD, USA

9 2. Department of Chemical and Biochemical Engineering, Iowa Technology Institute, Center for  
10 Global and Regional Environmental Research, University of Iowa, USA

11 3. STI, Universities Space Research Association (USRA), Huntsville, AL, USA

12 4. NASA Marshall Space Flight Center, Huntsville, AL, USA  
13

14 \* Correspondence:

15 Zhanqing Li (zhanqing@umd.edu) and Jing Wei (weijing\_rs@163.com; weijing@umd.edu)

16 **Abstract**

17 Gaseous pollutants at the ground level seriously threaten the urban air quality environment and  
18 public health. There are few estimates of gaseous pollutants that are spatially and temporally  
19 resolved and continuous across China. This study takes advantage of big data and artificial  
20 intelligence technologies to generate seamless daily maps of three major ambient pollutant gases,  
21 i.e., NO<sub>2</sub>, SO<sub>2</sub>, and CO, across China from 2013 to 2020 at a uniform spatial resolution of 10 km.  
22 Cross-validation between our estimates and ground observations illustrated a high data quality on a  
23 daily basis for surface NO<sub>2</sub>, SO<sub>2</sub>, and CO concentrations, with mean coefficients of determination  
24 (root-mean-square errors) of 0.84 (7.99 μg/m<sup>3</sup>), 0.84 (10.7 μg/m<sup>3</sup>), and 0.80 (0.29 mg/m<sup>3</sup>),  
25 respectively. We found that the COVID-19 lockdown had sustained impacts on gaseous pollutants,  
26 where surface CO recovered to its normal level in China on around the 34<sup>th</sup> day after the Lunar New  
27 Year, while surface SO<sub>2</sub> and NO<sub>2</sub> rebounded more than twice slower due to more CO emissions  
28 from increased residents' indoor cooking and atmospheric oxidation capacity. Surface NO<sub>2</sub>, SO<sub>2</sub>,  
29 and CO reached their peak annual concentrations of 21.3 ± 8.8 μg/m<sup>3</sup>, 23.1 ± 13.3 μg/m<sup>3</sup>, and 1.01  
30 ± 0.29 mg/m<sup>3</sup> in 2013, then continuously declined over time by 12%, 55%, and 17%, respectively,  
31 until 2020. The declining rates were more prominent from 2013 to 2017 due to the sharper  
32 reductions in anthropogenic emissions but have slowed down in recent years. Nevertheless, people  
33 still suffer from high-frequency risk exposure to surface NO<sub>2</sub> in eastern China, while surface SO<sub>2</sub>  
34 and CO have almost reached the recommended air quality guidelines level since 2018, benefiting  
35 from the implemented stricter “ultra-low” emission standards. This reconstructed dataset of surface  
36 gaseous pollutants will benefit future (especially short-term) air pollution and environmental health-  
37 related studies.

## 38 **1. Introduction**

39 Air pollution has been a major environmental concern, affecting human health, weather, and climate  
40 (Anenberg et al., 2022; Kan et al., 2012; Li et al., 2017a; Murray et al., 2020; Orellano et al., 2020),  
41 thus drawing worldwide attention. The sources of air pollution are complex. They include natural  
42 sources such as wildfires and anthropogenic emissions, including pollutants discharged from  
43 industrial production [e.g., smoke/dust, sulfur oxides, nitrogen oxides (NO<sub>x</sub>), and volatile organic  
44 compounds (VOCs)], hazardous substances released from burning coal during heating seasons [e.g.,  
45 dust, sulfur dioxide (SO<sub>2</sub>), and carbon monoxide (CO)], and waste gases (e.g., CO, SO<sub>2</sub>, and NO<sub>x</sub>)  
46 generated by transportation, especially in big cities.

47  
48 Among various air pollutants, the following have been most widely recognized: particulate matter  
49 with diameters smaller than 2.5 μm and 10 μm (PM<sub>2.5</sub> and PM<sub>10</sub>) and gaseous pollutants [e.g.,  
50 ozone (O<sub>3</sub>), nitrogen dioxide (NO<sub>2</sub>), SO<sub>2</sub>, and CO, among others]. Many countries have built  
51 ground-based networks to monitor a variety of conventional pollutants in real time. China has  
52 experienced serious ambient air pollution for a long time, prompting the establishment of a large-  
53 scale air quality monitoring network (MEE, 2018a). Over the years, much effort has been made to  
54 model different species of air pollutants. Many studies focused on particulate matter in China have  
55 been carried out (Gao et al., 2022; Li et al., 2017b; Li et al., 2022b; Ma et al., 2022; Yang et al.,  
56 2022; Zhang et al., 2018). The global COVID-19 pandemic has motivated many attempts to  
57 estimate surface NO<sub>2</sub> concentrations from satellite-retrieved tropospheric NO<sub>2</sub> products (Tian et al.,  
58 2020; WHO, 2020), e.g., from the Ozone Monitoring Instrument (OMI) onboard the NASA Aura  
59 spacecraft and the TROPOspheric Monitoring Instrument (TROPOMI) onboard the Copernicus  
60 Sentinel-5 Precursor satellite, adopting different statistical regression (Chi et al., 2021; Qin et al.,  
61 2017; Zhang et al., 2018) and artificial intelligence (Chen et al., 2019; Chi et al., 2022; Dou et al.,  
62 2021; Liu, 2021; Wang et al., 2021; Zhan et al., 2018) models. By comparison, surface SO<sub>2</sub> and CO  
63 in China are less studied, limited by weaker signals and a lack of good-quality satellite tropospheric  
64 products (Han et al., 2022b; Li et al., 2020; Liu et al., 2019; Wang et al., 2021). Such studies still  
65 face more challenges, e.g., satellite data gaps and missing values that seriously limit their  
66 application and the neglect of spatiotemporal differences in air pollution in the modeling process. In

67 addition, most previous studies mainly focused on studying a single or a few species during  
68 relatively short observational periods.

69

70 In view of the above problems, the purpose of this paper is to reconstruct daily concentrations of  
71 three ambient gaseous pollutants (i.e., NO<sub>2</sub>, SO<sub>2</sub>, and CO) in China. To this end, relying on the  
72 dense national ground-based observation network and big data, including satellite remote sensing  
73 products, meteorological reanalysis, chemical model simulations, and emission inventories, we are  
74 capable of mapping three pollutant gases seamlessly (100% spatial coverage) on a daily basis at a  
75 uniform spatial resolution of 10 km since 2013 in China. Estimates were made using an extended  
76 and powerful machine-learning model incorporating spatiotemporal information, i.e., space-time  
77 extra-trees. Natural and anthropogenic effects on air pollution, including their physical mechanisms  
78 and chemical reactions, were accounted for in the modeling. Using this dataset, spatiotemporal  
79 variations of the gaseous pollutants, the impacts of environmental protection policies and the  
80 COVID-19 epidemic, and population risk exposure to gaseous pollution are investigated.

81

82 To date, we have combined the advantages of artificial intelligence and big data to construct a  
83 virtually complete set of major air quality parameters concerning both particulate and gaseous  
84 pollutants over a long period of time across China, including PM<sub>1</sub> (1 km, 2000–Present) (Wei et al.,  
85 2019), PM<sub>2.5</sub> (1 km, 2000–Present) (Wei et al., 2020; Wei et al., 2021a), PM<sub>10</sub> (1 km, 2000–Present)  
86 (Wei et al., 2021b), O<sub>3</sub> (10 km, 1979–Present) (Wei et al., 2022a; He et al., 2022b), and NO<sub>2</sub> (1 km,  
87 2019–Present) (Wei et al., 2022b), serving environmental, public health, economy, and other related  
88 research. This study is the continuation of our previous studies, which adds two new species of SO<sub>2</sub>  
89 and CO for the first time and also dates the data records of NO<sub>2</sub> back to 2013. Instead of devoting  
90 itself to a single pollutant, this study deals with all gaseous pollutants of compatible quality over the  
91 same period with the same spatial coverage and resolution. In particular, considering that there are  
92 few public datasets of these three gaseous pollutants with such spatiotemporal coverages focusing  
93 on the whole of China, this is highly valuable for the sake of studying their variations, relative  
94 proportions, and attribution of emission sources, as well as their diverse and joint effects of different  
95 pollutant species on public health.

96

## 97 **2. Materials and methods**

### 98 **2.1 Big data**

#### 99 **2.1.1 Ground-based measurements**

100 Hourly measurements of ground-level NO<sub>2</sub>, SO<sub>2</sub>, and CO concentrations from ~1600 reference-  
101 grade ground-based monitoring stations (Figure 1) collected from the China National  
102 Environmental Monitoring Centre (CNEMC) network were employed in the study. This network  
103 includes urban assessing stations, regional assessing stations, background stations, source impact  
104 stations, and traffic stations, set up in a reasonable overall layout that covers industrial (~14%),  
105 urban (~31%), suburban (~39%), and rural (~16%) areas to improve the spatial representations,  
106 continuity, and comparability of observations (HJ 664-2013) (MEE, 2013a). NO<sub>2</sub> is measured by  
107 chemiluminescence and differential optical absorption spectroscopy (DOAS), and SO<sub>2</sub> uses  
108 ultraviolet fluorescence and DOAS, while CO adopts non-dispersive infrared spectroscopy and gas  
109 filter correlation infrared spectroscopy. These measurements have been fully validated and have the  
110 same average error of indication of  $\pm 2\%$  F.S. for the three gaseous pollutants considered here, with  
111 additional quality-control checks such as zero and span noise and zero and span drift (HJ 193-2013  
112 and HJ 654-2013) (MEE, 2013b, 2013c). They have also been used as ground truth in almost all air  
113 pollutant modelling studies in China (Ma et al., 2022; Zhang et al., 2022a). All stations use the same  
114 technique to measure each gas routinely and continuously 24 hours a day at about the sea level  
115 without time series gaps. However, the reference state (i.e., observational conditions like  
116 temperature and pressure) changed from the standard condition (i.e., 273 K and 1013 hPa) to the  
117 room condition (i.e., 298 K and 1013 hPa) on 31 August 2018 (MEE, 2018a). We thus first  
118 converted observations of the three gaseous pollutants after this date to the uniform standard  
119 condition for consistency. Here, daily values for each air pollutant were averaged from at least 30%  
120 of valid hourly measurements at each station in each year from 2013 to 2020.

121

*[Please insert Figure 1 here]*

## 122 **2.1.2 Main predictors**

123 A new daily tropospheric NO<sub>2</sub> dataset at a horizontal resolution of 0.25° × 0.25° in China was  
124 employed, created using a developed framework integrating OMI/Aura Quality Assurance for  
125 Essential Climate Variables (QA4ECV) and Global Ozone Monitoring Experiment–2B (GOME-2B)  
126 offline tropospheric NO<sub>2</sub> retrievals passing quality controls (i.e., cloud fraction < 0.3, surface albedo  
127 < 0.3, and solar zenith angle < 85°) (He et al., 2020). The reconstructed tropospheric NO<sub>2</sub> agreed  
128 well (R = 0.75–0.85) with Multi-AXis Differential Optical Absorption Spectroscopy (MAX-DOAS)  
129 measurements. Through this data fusion, the daily spatial coverage of satellite tropospheric NO<sub>2</sub>  
130 was significantly improved in China (average = 87%). Areas with a small number of missing values  
131 were imputed via a nonparametric machine-learning model by regressing the conversion  
132 relationship with Copernicus Atmosphere Monitoring Service (CAMS) tropospheric NO<sub>2</sub>  
133 assimilations (0.75° × 0.75°), making sure that the interpolation was consistent with the OMI/Aura  
134 overpass time (Inness et al., 2019; Wang et al., 2020b). The gap-filled tropospheric NO<sub>2</sub> was  
135 reliable compared with measurements (R = 0.94–0.98) (Wei et al., 2022b). The above two-step gap-  
136 filling procedures allowed us to generate a daily seamless tropospheric NO<sub>2</sub> dataset that removes  
137 the effects of clouds from satellite observations.

138  
139 Here, the reconstructed daily seamless tropospheric NO<sub>2</sub>, together with CAMS daily ground-level  
140 NO<sub>2</sub> assimilations (0.75° × 0.75°) averaged from all 3-hourly data in a day and monthly NO<sub>x</sub>  
141 anthropogenic emissions (0.1° × 0.1°) (Inness et al., 2019), were used as the main predictors for  
142 estimating surface NO<sub>2</sub>. Limited by the quality of direct satellite observations, daily model-  
143 simulated SO<sub>2</sub> and CO surface mass concentrations, averaged from all available data in a day  
144 provided by one-hourly Modern-Era Retrospective Analysis for Research and Applications, version  
145 2 (MERRA-2, 0.625° × 0.5°), 3-hourly CAMS (0.75° × 0.75°), and 3-hourly Goddard Earth  
146 Observing System Forward-Processing (0.3125° × 0.25°) global reanalyses were used as main  
147 predictors to retrieve surface SO<sub>2</sub> and CO, together with CAMS monthly SO<sub>2</sub> and CO  
148 anthropogenic emissions.

149

### 150 **2.1.3 Auxiliary factors**

151 Meteorological factors have important diverse effects on air pollutants (He et al., 2017; Li et al.,  
152 2019), e.g., the boundary-layer height reflects their vertical distribution and variations (Li et al.,  
153 2017a; Seo et al., 2017); temperature, humidity, and pressure can affect their photochemical  
154 reactions (Li et al., 2019; Xu et al., 2011; Zhang et al., 2019a); and rainfall and wind can also  
155 influence their removal, accumulation, and transport (Dickerson et al., 2007; Li et al., 2019). Eight  
156 daily meteorological variables, provided by the ERA5-Land ( $0.1^\circ \times 0.1^\circ$ ) (Muñoz-Sabater et al.,  
157 2021) and ERA5 global reanalysis ( $0.25^\circ \times 0.25^\circ$ ) (Hersbach et al., 2020), were calculated (i.e.,  
158 accumulated for precipitation and evaporation while averaged for the others) from all hourly data in  
159 a day, used as auxiliary variables to improve the modelling of gaseous pollutants. Other auxiliary  
160 remote-sensing data used to describe land-use cover/change [i.e., Moderate Resolution Imaging  
161 Spectroradiometer (MODIS) normalized difference vegetation index (NDVI),  $0.05^\circ \times 0.05^\circ$ ] and  
162 population distribution density (i.e., LandScan<sup>TM</sup>, 1 km) were employed as inputs to the machine-  
163 learning model because they are highly related to the type of pollutant emission and amounts of  
164 anthropogenic emissions, as well as the surface terrain [i.e., Shuttle Radar Topography Mission  
165 (SRTM) digital elevation model (DEM), 90m], which can affect the transmission of air pollutants.  
166 Table S1 provides detailed information about all the data used in this study. All variables were  
167 aggregated or resampled into a  $0.1^\circ \times 0.1^\circ$  resolution for consistency.

168

### 169 **2.2 Pollutant gas modelling**

170 Here, the developed Space-Time Extra-Tree (STET) model, integrating spatiotemporal  
171 autocorrelations of and differences in air pollutants to the Extremely Randomized Trees (ERT) (Wei  
172 et al., 2022a), was extended to estimate surface gaseous pollutants, i.e., NO<sub>2</sub>, SO<sub>2</sub>, and CO. ERT is  
173 an ensemble machine-learning model based on the decision tree, capable of solving the  
174 nonparametric multivariable nonlinear regression problem. Ensemble learning can avoid the lack of  
175 learning ability of a single learner, greatly improving accuracy. The introduced randomness  
176 enhances the model's anti-noise ability and minimizes the sensitivity to outliers and  
177 multicollinearity issues. It can handle high latitude, discrete or continuous data without data  
178 normalization and is easy to implement and parallel. However, several limitations exist, e.g., it is

179 difficult to make predictions beyond the range of training data, and there will be an over-fitting  
180 issue on some regression problems with high noise. The training efficiency diminishes with  
181 increasing memory occupation when the number of decision trees is large (Geurts et al., 2006).

182  
183 Compared with traditional tree-based models (e.g., random forest), ERT has a stronger randomness  
184 which randomly selects a feature subset at each node split and randomly obtains the optimal branch  
185 attributes and thresholds. This helps to create more independent decision trees, further reducing  
186 model variance and improving training accuracy (Geurts et al., 2006). The STET model has been  
187 successfully applied in estimating high-quality surface O<sub>3</sub> in our previous study (Wei et al., 2022a).  
188 It is thus extended here to regress the nonlinear conversion relationships between ground-based  
189 measurements and the main predictors and auxiliary factors for other species of gaseous pollutants.  
190 For surface NO<sub>2</sub>, the STET model was applied to the main variables of the satellite tropospheric  
191 NO<sub>2</sub> column, modelled surface NO<sub>2</sub> mass, and NO<sub>x</sub> emissions, together with ancillary variables of  
192 the previously mentioned meteorological, surface, and population variables (Equation 1). For  
193 surface SO<sub>2</sub> (Equation 2) and CO (Equation 3), modelled surface SO<sub>2</sub> and CO concentrations and  
194 SO<sub>2</sub> and CO emissions were used as main predictors along with the same auxiliary variables as NO<sub>2</sub>  
195 to construct the STET models separately.

196  
197  $NO_{2(ijt)} \sim f_{STET}(SNO_{2(ijt)}, MNO_{2(ijt)}, ENO_{xijm}, Meteorology_{ijt}, NDVI_{ijm}, DEM_{ijy}, POP_{ijy}, P_s, P_t), \quad (1)$

198  $SO_{2(ijt)} \sim f_{STET}(MSO_{2(ijt)}, ESO_{2(ijm)}, Meteorology_{ijt}, NDVI_{ijm}, DEM_{ijy}, POP_{ijy}, P_s, P_t), \quad (2)$

199  $CO_{ijt} \sim f_{STET}(MCO_{ijt}, ECO_{ijm}, Meteorology_{ijt}, NDVI_{ijm}, DEM_{ijy}, POP_{ijy}, P_s, P_t), \quad (3)$

200  
201 where  $NO_{2(ijt)}$ ,  $SO_{2(ijt)}$ , and  $CO_{ijt}$  indicate daily ground-based NO<sub>2</sub>, SO<sub>2</sub>, and CO measurements at  
202 one grid  $(i, j)$  on the  $t$ th day of a year;  $SNO_{2(ijt)}$  indicates the daily satellite tropospheric NO<sub>2</sub> column  
203 at one grid  $(i, j)$  on the  $t$ th day of a year;  $MNO_{2(ijt)}$ ,  $MSO_{2(ijt)}$ , and  $MCO_{ijt}$  indicate daily model-  
204 simulated surface NO<sub>2</sub>, SO<sub>2</sub>, and CO concentrations at one grid  $(i, j)$  on the  $t$ th day of a year;  
205  $ENO_{xijm}$ ,  $ESO_{2(ijm)}$ , and  $ECO_{ijm}$  indicate monthly anthropogenic NO<sub>x</sub>, SO<sub>2</sub>, and CO emissions at one  
206 grid  $(i, j)$  in the  $m$ th month of a year;  $Meteorology_{ijt}$  represents each meteorological variable at one  
207 grid  $(i, j)$  on the  $t$ th day of a year;  $DEM_{ijy}$  and  $POP_{ijy}$  indicate the elevation and population at one



208 grid  $(i, j)$  of a year; and  $P_s$  and  $P_t$  indicate the space and time terms (Wei et al., 2022a).

209

### 210 **3. Results and discussion**

#### 211 **3.1 Seamless mapping of surface gaseous pollutants**

212 Using the constructed STET model, we generated daily 10 km resolution datasets with complete  
213 coverage (spatial coverage = 100%) for three ground-level gaseous pollutants from 2013 to 2020 in  
214 China, called ChinaHighNO<sub>2</sub>, ChinaHighSO<sub>2</sub>, and ChinaHighCO. Monthly and annual maps were  
215 generated by directly averaging daily data at each grid. They belong to a series of public long-term,  
216 full-coverage, high-resolution, and high-quality datasets of a variety of ground-level air pollutants  
217 for China [ChinaHighAirPollutants (CHAP)] developed by our team. Figure 2 shows spatial  
218 distributions of the three pollutant gases across China on a typical day (1 January 2018). The spatial  
219 patterns of these gaseous pollutants were consistent with those observed on the ground, especially  
220 in highly polluted areas, e.g., severe surface NO<sub>2</sub> pollution in the North China Plain (NCP) and high  
221 surface SO<sub>2</sub> emissions in Shanxi Province. The unique advantage of our dataset is that it can  
222 provide valuable gaseous pollutant information on a daily basis at locations in China where ground  
223 measurements are not available. This addresses the major issues of scanning gaps and numerous  
224 missing values in satellite remote sensing retrievals at cloudy locations, e.g., the average spatial  
225 coverage of the official OMI/Aura daily tropospheric NO<sub>2</sub> product is only 42% over the whole of  
226 China during the period 2013–2020 (Figure S1). Our dataset provides spatially complete coverage,  
227 significantly increasing daily satellite observations by 58%. In addition, reanalysis data do not  
228 simulate surface masses of gaseous pollutants well, underestimating them compared to our results  
229 and ground-based observations in China (Figure S2). This is especially so for SO<sub>2</sub>, where high-  
230 pollution hot spots are easily misidentified. Validation illustrates that our regressed results for  
231 surface NO<sub>2</sub>, SO<sub>2</sub>, and CO agree better with ground measurements than modelled results (slopes are  
232 close to 1, and correlations > 0.93), 1.9–6.4 times stronger in slope, 1.3–3.5 times higher in  
233 correlation, but 5.9–7.7 times smaller in differences (Figure S3). This shows that our model can take  
234 advantage of big data to significantly correct and reconstruct gaseous simulation results via data  
235 mining using machine learning.

236

*[Please insert Figure 2 here]*

237 Figure 3 shows annual and seasonal maps for each gas pollutant during the period 2013–2020  
238 across China. Multi-year mean surface NO<sub>2</sub>, SO<sub>2</sub>, and CO concentrations were  $20.3 \pm 4.7 \mu\text{g}/\text{m}^3$ ,  
239  $16.2 \pm 7.7 \mu\text{g}/\text{m}^3$ , and  $0.86 \pm 0.22 \text{ mg}/\text{m}^3$ , respectively. Pollutant gases varied significantly in space  
240 across China, where high surface NO<sub>2</sub> levels were mainly distributed in typical urban  
241 agglomerations, e.g., the Beijing-Tianjin-Hebei (BTH) region, the Yangtze River and Pearl River  
242 Deltas (YRD and PRD), and scattered large cities with intensive human activities and highly  
243 developed transportation systems (e.g., Urumqi, Chengdu, Xi'an, and Wuhan, among others). High  
244 surface SO<sub>2</sub> concentrations were mainly observed in northern China (e.g., Shanxi, Hebei, and  
245 Shandong Provinces), associated with combustion emissions from anthropogenic sources, and the  
246 Yunnan Guizhou Plateau in southwest China, likely associated with emissions from volcanic  
247 eruptions. By contrast, except in some areas in central China (e.g., Shanxi and Hebei), surface CO  
248 concentrations were overall low.

249

250 Significant differences in spatial patterns were seen at the seasonal level. Surface NO<sub>2</sub>, SO<sub>2</sub>, and CO  
251 in summer (average =  $15.9 \pm 4.7 \mu\text{g}/\text{m}^3$ ,  $22.9 \pm 13.4 \mu\text{g}/\text{m}^3$ , and  $1.1 \pm 0.3 \text{ mg}/\text{m}^3$ , respectively) were  
252 the lowest, thanks to favorable meteorological conditions, e.g., abundant precipitation and high air  
253 humidity conducive to flushing and scavenging of different air pollutants (Yoo et al., 2014). Strong  
254 sunlight and high temperature also accelerate the photochemical reactions of NO<sub>2</sub> loss (Shah et al.,  
255 2020). Pollution levels were highest in winter, with average values increasing by ~1.5–1.9 times  
256 those in summer. This difference was much larger in central and eastern China, e.g., 2.3–3.4 times  
257 higher in the BTH due to large amounts of direct NO<sub>x</sub>, SO<sub>2</sub>, and CO emissions from burning coal  
258 for heating in winter in northern China. The spatial patterns of the three gaseous pollutants were  
259 similar in spring and autumn.

260

*[Please insert Figure 3 here]*

## 261 **3.2 Changes in gaseous pollution and exposure risk**

### 262 **3.2.1 Short-term epidemic effects on air quality**

263 Many studies have focused on the effects of the COVID-19 epidemic on air quality (WHO, 2020).

264 Most of them were done using ground-based observations (Huang et al., 2020; Su et al., 2020),

265 tropospheric gas columns (Field et al., 2021; Levelt et al., 2022), or retrieved surface masses  
266 (Cooper et al., 2022; Ling and Li, 2021). The resulting conclusions could be affected by insufficient  
267 spatial representation due to the uneven distribution of ground monitors or a large number of  
268 missing values in space due to the influence of clouds. The unique advantage of our seamless day-  
269 to-day gaseous pollutant dataset can make up for these shortcomings, allowing us to assess the  
270 changes more accurately and quantitatively in gaseous pollutants during the epidemic.

271

272 We first compared the spatial differences in monthly relative differences from February to April  
273 between 2020 and 2019 in China (Figure 4). In February, surface NO<sub>2</sub> sharply reduced in China,  
274 especially in key urban agglomerations and megacities, showing relative changes of greater than  
275 50%. A significant decrease in surface SO<sub>2</sub> (> 40%) was observed in northern areas where heavy  
276 industry is the mainstay in China (e.g., Tianjin, Hebei, and Shandong), while little change was seen  
277 in southern China. Surface CO also showed drastic decreases, but the amplitude was smaller than  
278 the other two gaseous pollutants. These were attributed to extensive plant closures and traffic  
279 controls due to the lockdown, which started at the end of January 2020, significantly reducing  
280 anthropogenic NO<sub>x</sub>, SO<sub>2</sub>, and CO emissions (Ding et al., 2020; Yang et al., 2022; Zheng et al.,  
281 2021). In March, surface NO<sub>2</sub> was still generally lower than the historical level in most eastern  
282 areas, especially in areas where the epidemic was severe, i.e., Wuhan, Hubei Province, and its  
283 surrounding areas. The decrease in surface SO<sub>2</sub> largely slowed by more than two times in the NCP  
284 and central China, while surface CO almost returned to normal levels in most areas in China. In  
285 April, surface NO<sub>2</sub> and SO<sub>2</sub> were comparable to historical concentrations (within  $\pm 10\%$ ), even  
286 increasing in some areas of southern and northeastern areas due to rebounding anthropogenic  
287 emissions (Ding et al., 2020), especially in Hubei Province, indicating that their surface levels were  
288 almost recovered.

289

*[Please insert Figure 4 here]*

290 Most previous studies have focused mainly on changes during the lockdown, with little attention  
291 paid to the recovery. We thus compared the time series of daily population-weighted concentrations  
292 of the three gaseous pollutants after the Lunar New Year between 2020 and 2019 in China (Figure

293 5). After the beginning of New Year's Eve, surface gaseous pollutants showed a significant decrease  
294 in both the normal and epidemic years due to the closure of factories, with decreasing  
295 anthropogenic emissions during the Spring Festival holiday. However, gaseous pollutants in the  
296 normal year rose rapidly after they fell to their lowest levels due to the return to work after the  
297 holidays. By contrast, their levels continued to decrease in 2020 and were lower than historical  
298 levels due to the sustained impacts of the strict lockdowns. They hit bottom in the 4<sup>th</sup> week after the  
299 Lunar New Year, then began to increase gradually. Surface NO<sub>2</sub> and SO<sub>2</sub> recovered in the middle of  
300 the 11<sup>th</sup> week (around the 72<sup>nd</sup> and 75<sup>th</sup> days) after the Lunar New Year (i.e., 2020 and 2019  
301 concentrations intersected and then alternately changed). However, surface CO levels recovered at  
302 the end of the 5<sup>th</sup> week (around the 34<sup>th</sup> day), more than twice faster than NO<sub>2</sub> and SO<sub>2</sub> levels. This  
303 is attributed to more CO emissions from increased residents' indoor cooking (Zheng et al., 2018),  
304 increased atmospheric oxidation capacity (Huang et al., 2020; Wei et al., 2022a), and a potentially  
305 higher sensitivity to temperature rises (Lin et al., 2021).

306 *[Please insert Figure 5 here]*

### 307 **3.2.2 Temporal variations and policy implications**

308 Figures S4-S6 show annual mean maps of each gaseous pollutant from 2013 to 2020 in China.  
309 Surface NO<sub>2</sub>, SO<sub>2</sub>, and CO changed greatly, peaking in 2013, with average values of  $21.3 \pm 8.8$   
310  $\mu\text{g}/\text{m}^3$ ,  $23.1 \pm 13.3 \mu\text{g}/\text{m}^3$ , and  $1.01 \pm 0.29 \text{ mg}/\text{m}^3$ , respectively. They reached their lowest levels in  
311 2020, particularly due to the noticeable effects of the COVID-19 epidemic. In general, national  
312 ambient NO<sub>2</sub>, SO<sub>2</sub>, and CO concentrations decreased by approximately 12%, 55%, and 17% from  
313 2013 to 2020, respectively. Large seasonal differences were observed in the amplitude of gaseous  
314 pollutant (Figure 6), e.g., surface NO<sub>2</sub> decreased the most in winter, especially in the three urban  
315 agglomerations ( $\downarrow 24\text{--}31\%$ ), changing the least in autumn (especially in the YRD). Surface SO<sub>2</sub>  
316 showed much larger decreases in all seasons, especially during the cold seasons ( $\downarrow 55\text{--}81\%$ ), due to  
317 the implementation of stricter “ultra-low” emission standards (Li et al., 2022a; Zhang et al., 2019b).  
318 Surface CO had similar seasonal changes as SO<sub>2</sub> but 1.5–3.3 times smaller in amplitude.

319 *[Please insert Figure 6 here]*

320 To better investigate the spatiotemporal variations of ambient gaseous pollution, we calculated  
321 linear trends and significance levels using monthly anomalies by removing seasonal cycles. Most of  
322 China showed significant decreasing trends, with average annual rates of  $0.23 \mu\text{g}/\text{m}^3$ ,  $2.01 \mu\text{g}/\text{m}^3$ ,  
323 and  $0.05 \text{mg}/\text{m}^3$  for surface  $\text{NO}_2$ ,  $\text{SO}_2$ , and  $\text{CO}$  ( $p < 0.001$ ), respectively (Figure 7), especially in  
324 three urban agglomerations and large cities (e.g., Wuhan and Chengdu). The largest downward  
325 trends mainly occurred in northern and central China, especially in the BTH (Table 3). This is  
326 mainly due to the change in fuel for heating from coal to gas widespread across China in winter  
327 (Wang et al., 2020a), greatly reducing emissions of precursor gases (Koukouli et al., 2018).  
328 Increasing trends of surface  $\text{NO}_2$  were, however, found in Ningxia and Shanxi Provinces in central  
329 China due to increased traffic emissions and new coal-burning power plants in underdeveloped  
330 areas without strict regulations on  $\text{NO}_x$  emissions (Li et al., 2022a; Maji and Sarkar, 2020; Van Der  
331 A et al., 2017).

332

333 We then divided the study period into three periods to investigate the impact of major  
334 environmental protection policies on air quality implemented in China (Figure 7). During the Clear  
335 Air Action Plan (CAAP, 2013–2017), the rates of decrease for surface  $\text{NO}_2$ ,  $\text{SO}_2$ , and  $\text{CO}$   
336 accelerated in most populated areas in China, especially urban areas. This was due to dramatic  
337 reductions in main pollutant emissions like  $\text{SO}_2$  and  $\text{NO}_x$  (by 59% and 21%, respectively) through  
338 the upgrading of key industries, industrial structure adjustments, and coal-fired boiler remediation  
339 (Zhang et al., 2019b). In addition, the majority of gaseous pollutants had dropped continuously  
340 during the Blue Sky Defense War (BSDW, 2018–2020), benefiting from continuous reductions in  
341 total air pollutant emissions and the impacts of COVID-19 (Jiang et al., 2021; Zheng et al., 2021).  
342 However, areas with trends passing the significance level sharply shrank, especially for surface  $\text{SO}_2$ .

343

344 During the 13<sup>th</sup> Five-Year-Plan (FYP, 2016–2020), the decreasing trends of the three gaseous  
345 pollutants across China slowed down compared to those during CAAP. Large decreases in surface  
346  $\text{NO}_2$  were mainly found in the BTH region and Henan Province, while slightly increasing trends  
347 occurred in southern China. Surface  $\text{SO}_2$  significantly decreased in most areas, where a greater  
348 downward trend was observed in Shanxi Province, mainly due to the reduction in coal consumption

349 thanks to a strengthened clean-heating policy (Lee et al., 2021). Surface CO also continuously  
350 decreased, more rapidly in central China but less rapidly elsewhere. The continuous decline in  
351 gaseous pollutants is due to the binding reductions in total emissions of major pollutants like NO<sub>x</sub>  
352 (↓71%) and SO<sub>2</sub> (↓48%) in China (Wan et al., 2022; Wu et al., 2022c).

353 *[Please insert Figure 7 here]*

### 354 **3.2.3 Population-risk exposure to gaseous pollution**

355 With the daily seamless datasets, we can evaluate the spatial and temporal variations of short-term  
356 population-risk exposure to the three gaseous pollutants by calculating the number of days in a  
357 given year exceeding the new recommended short-term minimum interim target (IT1) and desired  
358 air quality guidelines (AQG) level defined by the WHO in 2021 (WHO, 2021). The area exceeding  
359 the recommended levels (i.e., daily NO<sub>2</sub> > 120 µg/m<sup>3</sup>, SO<sub>2</sub> > 125 µg/m<sup>3</sup>, and CO > 7 mg/m<sup>3</sup>) was  
360 generally small in eastern China (Figure S7). High NO<sub>2</sub>-exposure risks were mainly found in  
361 Beijing and Hebei Province and a handful of big cities (e.g., Jinan, Wuhan, Shanghai, and  
362 Guangzhou), while high SO<sub>2</sub>-exposure risks were mainly observed in Hebei, Shandong, and  
363 Shaanxi Provinces. The risk of high CO pollution was small, only found in some scattered areas in  
364 the NCP. In general, both the area and the possibility of occurrence exposure to high pollution has  
365 gradually decreased over time, almost disappearing since 2018.

366  
367 By contrast, most areas of eastern China had a surface NO<sub>2</sub> exposure exceeding the AQG level  
368 (Figure 8), especially in the north and economically developed areas in the south (proportion >  
369 80%). Both the extent and intensity are decreasing over time, but it is still a problem, suggesting  
370 that stronger NO<sub>x</sub> controls are needed in the future. Most of the main air pollution transmission belt  
371 in China (i.e., the “2 + 26” cities, Figure 1) had surface SO<sub>2</sub> levels exceeding the AQG level at the  
372 beginning of the study period. Thanks to strict control measures, these polluted areas sharply  
373 decreased after 2015, almost disappearing in 2020. Controlling CO was much more successful in  
374 China, with less than 10% of the days in the BTH exceeding the acceptable standard in the early  
375 part of the study period. Most areas have reached the CO AQG level since 2018.

376 *[Please insert Figure 8 here]*

377 Figure 9 shows the percentage of days with pollution levels exceeding WHO air quality standards in  
378 three key regions. BTH was the only region experiencing high NO<sub>2</sub> and SO<sub>2</sub> exposure risks (i.e.,  
379 daily mean > IT1), dropping to zero since 2017 and 2016, while YRD and PRD had no high risks of  
380 exposure to the three gaseous pollutants (Figure 9a-b). There was also no regional high CO-  
381 pollution risk (Figure 9c). However, although declining continuously, regional surface NO<sub>2</sub> levels  
382 failed to meet the short-term AQG level in 2020, with 61–73% of the days exceeding the AQG level.  
383 More efforts toward mitigating NO<sub>2</sub> levels in these key regions are thus needed. Continual  
384 decreases in the number of days above the AQG level were also observed in surface SO<sub>2</sub>, reducing  
385 to near zero in 2014, 2016, and 2018 in the PRD, YRD, and BTH, respectively. Less than 3% of the  
386 days in the BTH and YRD had surface CO levels exceeding the AQG level. Surface CO levels were  
387 always below the AQG level in the PRD.

388 *[Please insert Figure 9 here]*

### 389 **3.3 Data quality assessment**

390 Here, the widely used out-of-sample 10-fold cross-validation (10-CV) method was adopted to  
391 evaluate the overall estimation accuracy of gaseous pollutants (Rodriguez et al., 2010; Wei et al.,  
392 2022a). An additional out-of-station 10-CV approach was used to validate the prediction accuracy  
393 of gaseous pollutants, performed based on measurements from ground monitoring stations. These  
394 measurements were randomly divided into ten subsets, of which data samples from nine subsets  
395 were used for model training and the remaining subset for model validation. This was done 10 times,  
396 in turn, to ensure that data from all stations were tested. This procedure generates independent  
397 training samples and test samples made in different locations, used to indicate the spatial prediction  
398 ability of the model in areas where ground-based measurements are unavailable (Wei et al., 2022a;  
399 Wu et al., 2021).

400

#### 401 **3.3.1 Estimate and prediction accuracy**

402 Figure 10 shows the CV results of all daily estimates and predictions for ground-level NO<sub>2</sub>, SO<sub>2</sub>,  
403 and CO concentrations from 2013 to 2020 in China (sample size:  $N \approx 3.6$  million). Surface NO<sub>2</sub>  
404 and SO<sub>2</sub> concentrations mainly fell in the range of 200 to 500  $\mu\text{g}/\text{m}^3$ . Daily estimates were highly

405 correlated to observations, with the same coefficients of determination ( $R^2 = 0.84$ ) and slopes close  
406 to 1 (0.86 and 0.84, respectively). Average root-mean-square error (RMSE) [mean absolute error  
407 (MAE)] values of surface  $\text{NO}_2$  and  $\text{SO}_2$  estimates were 7.99 (5.34) and 10.07 (4.68)  $\mu\text{g}/\text{m}^3$ , and  
408 normalized RMSE (NRMSE) values were 0.25 and 0.51, respectively. Most daily CO observations  
409 were less than 10  $\text{mg}/\text{m}^3$ , agreeing well with our daily estimates ( $R^2 = 0.80$ , slope = 0.79), and the  
410 average RMSE (MAE) and NRMSE values were 0.29 (0.16)  $\text{mg}/\text{m}^3$  and 0.3. Compared to  
411 estimation accuracies (Figure 10a-c), prediction accuracies slightly decreased, which is acceptable  
412 considering the weak signals of trace gases. Daily surface  $\text{SO}_2$ ,  $\text{NO}_2$ , and CO predictions (Figure  
413 10d-f) agree well with ground measurements, with spatial  $R^2$  values of 0.70, 0.68, and 0.61,  
414 respectively. Their respective RMSE (MAE) values were 14.28 (8.1)  $\mu\text{g}/\text{m}^3$ , 11.57 (7.06)  $\mu\text{g}/\text{m}^3$ ,  
415 and 0.42 (0.24)  $\text{mg}/\text{m}^3$ , and NRMSE values were 0.35, 0.71, and 0.42, respectively, representing the  
416 accuracy for areas without ground monitoring stations.

417 *[Please insert Figure 10 here]*

418 The performance of our air pollution modelling was also evaluated on an annual basis, showing that  
419 our model works well in estimating and predicting the concentrations of different surface gaseous  
420 pollutants in different years (Table 1). The model performance has continuously improved over time,  
421 as indicated by increasing correlations and decreasing uncertainties. This is because of the  
422 increasing density of ground stations (especially in the suburban areas of cities) and updated quality  
423 control of measurements, e.g., improving the sampling flow calibration of monitoring instruments,  
424 flow calibration of dynamic calibrators, and revision of precision/accuracy review and data validity  
425 judgment (HJ 818-2018) (MEE, 2018b). This has led to an increase in the number of data samples  
426 (e.g., from 169 thousand in 2013 to more than 522 thousand in 2020) and improvement in their  
427 quality.

428 *[Please insert Table 1 here]*

429 Figure 11 shows the spatial validation of estimated daily pollutant gases across China. In general,  
430 our model works well at the site scale, with average CV- $R^2$  values of 0.77, 0.72, and 0.72, and  
431 NRMSE values of 0.25, 0.43, and 0.26 for surface  $\text{NO}_2$ ,  $\text{SO}_2$ , and CO, respectively. In addition,



432 approximately 93%, 80%, and 84% of the stations had at least moderate agreements ( $CV-R^2 > 0.6$ )  
433 between our estimates and ground measurements. Except for some scattered sites, the estimation  
434 uncertainties were generally less than 0.3, 0.5, and 0.3 in more than 80%, 77%, and 76% of the  
435 stations for the above three gaseous pollutant species, respectively.

436 *[Please insert Figure 11 here]*

437 Figure 12 shows the temporal validation of ground-level gaseous pollutants as a function of ground  
438 measurements in China. On the monthly scale (Figure 12a-c), we collected a total of ~119,000  
439 matched samples of the three gaseous pollutants. Accuracies significantly improved, with increasing  
440  $R^2$  (decreasing RMSE) values of 0.93 ( $4.41 \mu\text{g}/\text{m}^3$ ), 0.97 ( $4.03 \mu\text{g}/\text{m}^3$ ), and 0.94 ( $0.13 \text{mg}/\text{m}^3$ ) for  
441 surface  $\text{NO}_2$ ,  $\text{SO}_2$ , and  $\text{CO}$ , respectively. On the annual scale (Figure 12d-f), more than ~10,000  
442 matched samples were collected, showing better agreement with observations (e.g.,  $R^2 = 0.94, 0.98,$   
443 and  $0.97$ ) and lower uncertainties (e.g.,  $\text{RMSE} = 3.06 \mu\text{g}/\text{m}^3, 2.46 \mu\text{g}/\text{m}^3,$  and  $0.07 \text{mg}/\text{m}^3$ ) for the  
444 above three gaseous pollutants, respectively.

445 *[Please insert Figure 12 here]*

### 446 **3.3.2 Comparison with previous studies**

447 We compared our results with those from previous studies on the estimation of the three gaseous  
448 pollutants using different developed models focusing on the whole of China. Here, only those  
449 studies applying the same out-of-sample cross-validation approach against ground-based  
450 measurements collected from the same CNEMC network were selected (Table 2). The statistics  
451 shown in the table come from the publications themselves because their generated datasets are not  
452 publicly available. We have applied the same validation method and ground measurements as those  
453 used in the previous studies. Most generated surface  $\text{NO}_2$  datasets had numerous missing values in  
454 space limited by direct OMI/Aura satellite observations at spatial resolutions from  $0.125^\circ \times 0.125^\circ$   
455 to  $0.25^\circ \times 0.25^\circ$  (Chen et al., 2019; Chi et al., 2021; Dou et al., 2021; Xu et al., 2019; Zhan et al.,  
456 2018). Some studies improved the spatial resolution by introducing  $\text{NO}_2$  data from the recently  
457 launched Sentinel-5 TROPOMI satellite, but data are only available from October 2018 onward  
458 (Chi et al., 2022; Liu, 2021; Wang et al., 2021; Wei et al., 2022b). Surface  $\text{SO}_2$  estimated from an

459 SO<sub>2</sub> emission inventory and surface CO from Measurement of Pollution in the Troposphere  
460 (MOPITT) and TROPOMI retrievals have a much lower data quality, with smaller R<sup>2</sup> values by 12–  
461 57% and larger RMSE values by 41–47% against ground measurements compared to ours (Li et al.,  
462 2020; Liu et al., 2019; Wang et al., 2021). Overall, our gaseous pollutant datasets are superior to  
463 those from previous studies in terms of overall accuracy, spatial coverage, and length of data  
464 records.

465 *[Please insert Table 2 here]*

### 466 **3.4 Successful applications**

467 Our surface gaseous pollutant datasets have been freely available to the public online since March  
468 2021 (See data availability). A large number of studies have used the three gaseous pollutant  
469 datasets generated in this study to study their single or joint impacts on environmental health from  
470 both long-term and short-term perspectives, benefiting from the unique daily spatially seamless  
471 coverage. For example, a nearly linear relationship between long-term ambient NO<sub>2</sub> and adult  
472 mortality in China was observed (Zhang et al., 2022b); ambient NO<sub>2</sub> hindered the survival of  
473 middle-aged and elderly people (Wang et al., 2023) while acute exposure to ambient SO<sub>2</sub> increased  
474 the risk of asthma mortality in China (Li et al., 2023b; Liu et al., 2022b; Liu et al., 2023). Long-  
475 term SO<sub>2</sub> and CO exposure can increase the incidence rate of visual impairment in children in China  
476 (Chen et al., 2022a), and short-term exposure to ambient CO can significantly increase the  
477 probability of hospitalization for stroke sequelae (Wang et al., 2022b). Regional and national cohort  
478 studies have shown that exposure, especially short-term exposure, to multiple ambient gaseous  
479 (NO<sub>2</sub>, SO<sub>2</sub>, and CO) and particulate pollutants have negative effects of varying degrees on a variety  
480 of diseases, like all-cause mortality (Feng et al., 2023), dementia mortality (Liu et al., 2022a),  
481 myocardial infarction mortality (Ma et al., 2023), cause-specific cardiovascular disease (Xu et al.,  
482 2022a; Xu et al., 2022b), respiratory diseases (Li et al., 2023a), ischemic and hemorrhagic stroke  
483 (Cai et al., 2022; He et al., 2022a; Wu et al., 2022b; Xu et al., 2022c), metabolic syndrome (Guo et  
484 al., 2022; Han et al., 2022a), influenza-like illness (Lu et al., 2023), incident dyslipidemia (Hu et al.,  
485 2023), diabetes (Mei et al., 2023), blood pressure (Song et al., 2022; Wu et al., 2022a), renal/ kidney  
486 function (Li et al., 2022c; Li et al., 2023c), neurodevelopmental delay (Su et al., 2022), serum liver

487 enzymes (Li et al., 2022d), overweight and obesity (Chen et al., 2022b), insomnia (Xu et al., 2021),  
488 and sleep quality (Wang et al., 2022a). These studies attest well to the value of the CHAP dataset  
489 regarding current and future public health issues, among others.

490

#### 491 **4. Summary and conclusions**

492 Exposure to gaseous pollution is detrimental to human health, a major public concern in heavily  
493 polluted regions like China, where ground-based observations are not as rich as in major developed  
494 countries. Moreover, pollutants travel long distances, affecting large downstream regions. To  
495 remedy such limitations, this study applied the machine-learning model called Space-Time Extra-  
496 Tree to estimate ambient gaseous pollutants across China, with extensive input variables measured  
497 by monitors and satellites, and models. Daily 10 km resolution (approximately  $0.1^\circ \times 0.1^\circ$ ) seamless  
498 (spatial coverage = 100%) datasets for ground-level NO<sub>2</sub>, SO<sub>2</sub>, and CO concentrations in China  
499 from 2013 to 2020 were generated. These datasets were cross-evaluated in terms of overall  
500 accuracy and predictive ability at different spatiotemporal levels. National daily estimates  
501 (predictions) of surface NO<sub>2</sub>, SO<sub>2</sub>, and CO were highly consistent with ground measurements, with  
502 average out-of-sample (out-of-station) CV-R<sup>2</sup> values of 0.84 (0.68), 0.84 (0.7), and 0.8 (0.61), and  
503 RMSEs of 7.99 (11.57)  $\mu\text{g}/\text{m}^3$ , 10.7 (14.28)  $\mu\text{g}/\text{m}^3$ , and 0.29 (0.42)  $\text{mg}/\text{m}^3$ , respectively.

504

505 Ambient pollutant gases varied significantly in space and time, with high levels mainly found in the  
506 North China Plain, especially in winter, due to more anthropogenic emissions, such as coal burning  
507 for heating. All gaseous pollutants sharply declined in China during the COVID-19 outbreak, while  
508 large differences were observed during their recovery times. For example, surface CO was the first  
509 to return to its historical level within the fifth week after the Lunar New Year in 2020, about twice  
510 faster as surface NO<sub>2</sub> and SO<sub>2</sub> levels. This is attributed to more home cooking and enhanced  
511 atmospheric oxidation. Temporally, surface NO<sub>2</sub>, SO<sub>2</sub>, and CO levels in China gradually decreased  
512 from peaks in 2013 (average =  $21.3 \pm 8.8 \mu\text{g}/\text{m}^3$ ,  $23.1 \pm 13.3 \mu\text{g}/\text{m}^3$ , and  $1.01 \pm 0.29 \text{mg}/\text{m}^3$ ,  
513 respectively), with annual rates of decrease of  $0.23 \mu\text{g}/\text{m}^3$ ,  $2.01 \mu\text{g}/\text{m}^3$ , and  $0.05 \text{mg}/\text{m}^3$ ,  
514 respectively ( $p < 0.001$ ), until 2020. Improvements in air quality have been made in the last eight  
515 years, thanks to the implementation of a series of environmental protection policies, greatly

516 reducing pollutant emissions. In addition, both the areal extents of regions experiencing gaseous  
517 pollution and the probability of gaseous pollution occurring have gradually decreased over time,  
518 especially for surface CO and SO<sub>2</sub>, which have almost reached the short-term air quality guidelines  
519 level recommended by the WHO in most areas in China in 2020. This high-quality daily seamless  
520 dataset of gaseous pollutants will benefit future environmental and health-related studies focused on  
521 China, especially studies investigating short-term air pollution exposure.

522

523 Although a lot of new and/or useful data and analyses are presented in this study, they still suffer  
524 from some limitations. For example, our estimated surface SO<sub>2</sub> and CO concentrations should have  
525 larger uncertainties than those of NO<sub>2</sub> since model simulations instead of satellite retrievals are  
526 supplemented during modelling to compensate for the lack of data in China. However, these data  
527 often have large biases in the remote regions with few observations as in western China (Li et al.,  
528 2022b), as the surface measurements from MEE are mainly over eastern China. More influential  
529 factors stemming from regional economic and development differences, and more parameters  
530 describing the complex meteorological system (e.g., winds at 850 hPa and the pressure system in  
531 the mid-troposphere) need to be considered in developing more powerful artificial intelligence  
532 models, which could be helpful in improving the accuracy of air pollutant retrievals. The  
533 spatiotemporal resolutions of gaseous pollutants will be further improved by integrating information  
534 from polar-orbiting and geostationary satellites to investigate diurnal variations. In a future study,  
535 we will also reconstruct data records over the last two decades and investigate their long-term  
536 spatiotemporal variations, filling the gap of missing observations. This will help us understand their  
537 formation mechanisms and impacts on fine particulate matter and ozone pollution in China.

538

### 539 **Data availability**

540 CNEMC measurements of gaseous pollutants are available at <http://www.cnemc.cn>. The  
541 reconstructed OMI/Aura tropospheric NO<sub>2</sub> product is available at  
542 <https://doi.org/10.6084/m9.figshare.13126847>. MODIS series products and the MERRA-2  
543 reanalysis are available at <https://search.earthdata.nasa.gov/>. The SRTM DEM is available at  
544 <https://www2.jpl.nasa.gov/srtm/>, and LandScan<sup>TM</sup> population information is available at

545 <https://landscan.ornl.gov/>. The ERA5 reanalysis is available at <https://cds.climate.copernicus.eu/>,  
546 GEOS CF data are available at <https://portal.nccs.nasa.gov/datashare/gmao/>, and the CAMS  
547 reanalysis and emission inventory are available at <https://ads.atmosphere.copernicus.eu/>.

548

549 The ChinaHighAirPollutants (CHAP) dataset is open access and freely available at [https://weijing-](https://weijing-rs.github.io/product.html)  
550 [rs.github.io/product.html](https://weijing-rs.github.io/product.html). The ChinaHighNO<sub>2</sub> dataset is available at  
551 <https://doi.org/10.5281/zenodo.4641542>, the ChinaHighSO<sub>2</sub> dataset is available at  
552 <https://doi.org/10.5281/zenodo.4641538>, and the ChinaHighCO dataset is available at  
553 <https://doi.org/10.5281/zenodo.4641530>.

554

#### 555 **Author contributions**

556 JiW and ZL designed the study. JiW performed the research and wrote the initial draft of this paper.  
557 ZL, JuW, CL, and PG reviewed and edited the paper. MC copyedited the article. All authors made  
558 substantial contributions to this work.

559

#### 560 **Competing interests**

561 The authors declare that they have no conflict of interest.

562

#### 563 **Acknowledgments**

564 JiW, ZL, and JuW were supported by NASA Earth Sciences' Applied Science Programs  
565 (80NSSC21K1980 and 80NSSC19K0950). PG was supported by NASA's Research Opportunities  
566 in Space and Earth Science (ROSES-2020), Program Element A.38: Health and Air Quality  
567 Applied Sciences Team.

568 **References**

- 569 Anenberg, S. C., Mohegh, A., Goldberg, D. L., Kerr, G. H., Brauer, M., Burkart, K., Hystad, P.,  
570 Larkin, A., Wozniak, S., and Lamsal, L.: Long-term trends in urban NO<sub>2</sub>  
571 concentrations and associated paediatric asthma incidence: estimates from global datasets, *The*  
572 *Lancet Planetary Health*, 6, e49-e58, [https://doi.org/10.1016/S2542-5196\(21\)00255-2](https://doi.org/10.1016/S2542-5196(21)00255-2), 2022.
- 573 Cai, M., Zhang, S., Lin, X., Qian, Z., McMillin, S. E., Yang, Y., Zhang, Z., Pan, J., and Lin, H.:  
574 Association of Ambient Particulate Matter Pollution of Different Sizes With In-Hospital Case  
575 Fatality Among Stroke Patients in China, *Neurology*, 10.1212/WNL.0000000000200546,  
576 <https://doi.org/10.1212/WNL.0000000000200546>, 2022.
- 577 Chen, L., Wei, J., Ma, T., Gao, D., Wang, X., Wen, B., Chen, M., Li, Y., Jiang, J., Wu, L., Li, W.,  
578 Liu, X., Song, Y., Guo, X., Dong, Y., and Ma, J.: Ambient gaseous pollutant exposure and  
579 incidence of visual impairment among children and adolescents: findings from a longitudinal,  
580 two-center cohort study in China, *Environmental Science and Pollution Research*,  
581 <https://doi.org/10.1007/s11356-022-20025-3>, 2022a.
- 582 Chen, L., Gao, D., Ma, T., Chen, M., Li, Y., Ma, Y., Wen, B., Jiang, J., Wang, X., Zhang, J., Chen, S.,  
583 Wu, L., Li, W., Liu, X., Guo, X., Huang, S., Wei, J., Song, Y., Ma, J., and Dong, Y.: Could  
584 greenness modify the effects of physical activity and air pollutants on overweight and obesity  
585 among children and adolescents?, *Science of The Total Environment*, 832, 155117,  
586 <https://doi.org/10.1016/j.scitotenv.2022.155117>, 2022b.
- 587 Chen, Z.-Y., Zhang, R., Zhang, T.-H., Ou, C.-Q., and Guo, Y.: A kriging-calibrated machine learning  
588 method for estimating daily ground-level NO<sub>2</sub> in mainland China, *Science of The Total*  
589 *Environment*, 690, 556-564, <https://doi.org/10.1016/j.scitotenv.2019.06.349>, 2019.
- 590 Chi, Y., Fan, M., Zhao, C., Sun, L., Yang, Y., Yang, X., and Tao, J.: Ground-level NO<sub>2</sub>  
591 concentration estimation based on OMI tropospheric NO<sub>2</sub> and its spatiotemporal  
592 characteristics in typical regions of China, *Atmospheric Research*, 264, 105821,  
593 <https://doi.org/10.1016/j.atmosres.2021.105821>, 2021.
- 594 Chi, Y., Fan, M., Zhao, C., Yang, Y., Fan, H., Yang, X., Yang, J., and Tao, J.: Machine learning-  
595 based estimation of ground-level NO<sub>2</sub> concentrations over China, *Science of The Total*  
596 *Environment*, 807, 150721, <https://doi.org/10.1016/j.scitotenv.2021.150721>, 2022.
- 597 Cooper, M. J., Martin, R. V., Hammer, M. S., Levelt, P. F., Veefkind, P., Lamsal, L. N., Krotkov, N.  
598 A., Brook, J. R., and McLinden, C. A.: Global fine-scale changes in ambient NO<sub>2</sub> during  
599 COVID-19 lockdowns, *Nature*, 601, 380-387, 10.1038/s41586-021-04229-0, 2022.
- 600 Dickerson, R. R., Li, C., Li, Z., Marufu, L. T., Stehr, J. W., McClure, B., Krotkov, N., Chen, H.,  
601 Wang, P., Xia, X., Ban, X., Gong, F., Yuan, J., and Yang, J.: Aircraft observations of dust and  
602 pollutants over northeast China: Insight into the meteorological mechanisms of transport,  
603 *Journal of Geophysical Research: Atmospheres*, 112, <https://doi.org/10.1029/2007JD008999>,  
604 2007.
- 605 Ding, J., van der A, R. J., Eskes, H. J., Mijling, B., Stavrou, T., van Geffen, J. H. G. M., and  
606 Veefkind, J. P.: NO<sub>x</sub> Emissions Reduction and Rebound in China Due to the COVID-19 Crisis,  
607 *Geophysical Research Letters*, 47, e2020GL089912, <https://doi.org/10.1029/2020GL089912>,  
608 2020.
- 609 Dou, X., Liao, C., Wang, H., Huang, Y., Tu, Y., Huang, X., Peng, Y., Zhu, B., Tan, J., Deng, Z., Wu,  
610 N., Sun, T., Ke, P., and Liu, Z.: Estimates of daily ground-level NO<sub>2</sub> concentrations in China  
611 based on Random Forest model integrated K-means, *Advances in Applied Energy*, 2, 100017,

612 <https://doi.org/10.1016/j.adapen.2021.100017>, 2021.

613 Feng, C., Yu, B., Fei, T., Jia, P., Dou, Q., and Yang, S.: Association between residential greenness  
614 and all-cause mortality and the joint mediation effect of air pollutants among old people with  
615 disability: A prospective cohort study, *Science of The Total Environment*, 858, 159604,  
616 <https://doi.org/10.1016/j.scitotenv.2022.159604>, 2023.

617 Field, R. D., Hickman, J. E., Geogdzhayev, I. V., Tsigaridis, K., and Bauer, S. E.: Changes in  
618 satellite retrievals of atmospheric composition over eastern China during the 2020 COVID-19  
619 lockdowns, *Atmospheric Chemistry and Physics*, 21, 18333-18350,  
620 <https://doi.org/10.5194/acp-21-18333-2021>, 2021.

621 Gao, J., Yang, Y., Wang, H., Wang, P., Li, H., Li, M., Ren, L., Yue, X., and Liao, H.: Fast climate  
622 responses to emission reductions in aerosol and ozone precursors in China during 2013–2017,  
623 *Atmospheric Chemistry and Physics*, 22, 7131-7142, [10.5194/acp-22-7131-2022](https://doi.org/10.5194/acp-22-7131-2022), 2022.

624 Geurts, P., Ernst, D., and Wehenkel, L.: Extremely Randomized Trees, *Machine Learning*, 36, 3--42,  
625 <https://doi.org/10.1007/s10994-006-6226-1>, 2006.

626 Guo, Q., Zhao, Y., Zhao, J., Bian, M., Qian, L., Xue, T., Zhang, J., and Duan, X.: Physical activity  
627 attenuated the associations between ambient air pollutants and metabolic syndrome (MetS): A  
628 nationwide study across 28 provinces, *Environmental Pollution*, 315, 120348,  
629 <https://doi.org/10.1016/j.envpol.2022.120348>, 2022.

630 Han, S., Zhang, F., Yu, H., Wei, J., Xue, L., Duan, Z., and Niu, Z.: Systemic inflammation  
631 accelerates the adverse effects of air pollution on metabolic syndrome: Findings from the  
632 China health and Retirement Longitudinal Study (CHARLS), *Environmental Research*, 215,  
633 114340, <https://doi.org/10.1016/j.envres.2022.114340>, 2022a.

634 Han, W., He, T. L., Tang, Z., Wang, M., Jones, D., and Jiang, Z.: A comparative analysis for a deep  
635 learning model (hyDL-CO v1.0) and Kalman filter to predict CO concentrations in China,  
636 *Geoscientific Model Development*, 15, 4225-4237, <https://doi.org/10.5194/gmd-15-4225-2022>,  
637 2022b.

638 He, F., Wei, J., Dong, Y., Liu, C., Zhao, K., Peng, W., Lu, Z., Zhang, B., Xue, F., Guo, X., and Jia,  
639 X.: Associations of ambient temperature with mortality for ischemic and hemorrhagic stroke  
640 and the modification effects of greenness in Shandong Province, China, *Science of The Total  
641 Environment*, 158046, <https://doi.org/10.1016/j.scitotenv.2022.158046>, 2022a.

642 He, J., Gong, S., Yu, Y., Yu, L., Wu, L., Mao, H., Song, C., Zhao, S., Liu, H., Li, X., and Li, R.: Air  
643 pollution characteristics and their relation to meteorological conditions during 2014–2015 in  
644 major Chinese cities, *Environmental Pollution*, 223, 484-496,  
645 <https://doi.org/10.1016/j.envpol.2017.01.050>, 2017.

646 He, L., Wei, J., Wang, Y., Shang, Q., Liu, J., Yin, Y., Frankenberg, C., Jiang, J. H., Li, Z., and Yung,  
647 Y. L.: Marked Impacts of Pollution Mitigation on Crop Yields in China, *Earth's Future*, 10,  
648 e2022EF002936, <https://doi.org/10.1029/2022EF002936>, 2022b.

649 He, Q., Qin, K., Cohen, J. B., Loyola, D., Li, D., Shi, J., and Xue, Y.: Spatially and temporally  
650 coherent reconstruction of tropospheric NO<sub>2</sub> over China combining OMI and GOME-2B  
651 measurements, *Environmental Research Letters*, 15, 125011, [https://doi.org/10.1088/1748-  
652 9326/abc7df](https://doi.org/10.1088/1748-9326/abc7df), 2020.

653 Hersbach, H., Bell, B., Berrisford, P., Hirahara, S., Horányi, A., Muñoz-Sabater, J., Nicolas, J.,  
654 Peubey, C., Radu, R., Schepers, D., Simmons, A., Soci, C., Abdalla, S., Abellan, X., Balsamo,  
655 G., Bechtold, P., Biavati, G., Bidlot, J., Bonavita, M., De Chiara, G., Dahlgren, P., Dee, D.,

656 Diamantakis, M., Dragani, R., Flemming, J., Forbes, R., Fuentes, M., Geer, A., Haimberger, L.,  
657 Healy, S., Hogan, R. J., Hólm, E., Janisková, M., Keeley, S., Laloyaux, P., Lopez, P., Lupu, C.,  
658 Radnoti, G., de Rosnay, P., Rozum, I., Vamborg, F., Villaume, S., and Thépaut, J.-N.: The  
659 ERA5 global reanalysis, *Quarterly Journal of the Royal Meteorological Society*, 146, 1999-  
660 2049, <https://doi.org/10.1002/qj.3803>, 2020.

661 Hu, M., Wei, J., Hu, Y., Guo, X., Li, Z., Liu, Y., Li, S., Xue, Y., Li, Y., Liu, M., Wang, L., and Liu,  
662 X.: Long-term effect of submicronic particulate matter (PM1) and intermodal particulate  
663 matter (PM1-2.5) on incident dyslipidemia in China: A nationwide 5-year cohort study,  
664 *Environmental Research*, 217, 114860, <https://doi.org/10.1016/j.envres.2022.114860>, 2023.

665 Huang, X., Ding, A., Gao, J., Zheng, B., Zhou, D., Qi, X., Tang, R., Wang, J., Ren, C., Nie, W., Chi,  
666 X., Xu, Z., Chen, L., Li, Y., Che, F., Pang, N., Wang, H., Tong, D., Qin, W., Cheng, W., Liu, W.,  
667 Fu, Q., Liu, B., Chai, F., Davis, S. J., Zhang, Q., and He, K.: Enhanced secondary pollution  
668 offset reduction of primary emissions during COVID-19 lockdown in China, *National Science*  
669 *Review*, 8, <https://doi.org/10.1093/nsr/nwaa137>, 2020.

670 Inness, A., Ades, M., Agustí-Panareda, A., Barré, J., Benedictow, A., Blechschmidt, A. M.,  
671 Dominguez, J. J., Engelen, R., Eskes, H., Flemming, J., Huijnen, V., Jones, L., Kipling, Z.,  
672 Massart, S., Parrington, M., Peuch, V. H., Razinger, M., Remy, S., Schulz, M., and Suttie, M.:  
673 The CAMS reanalysis of atmospheric composition, *Atmospheric Chemistry and Physics*, 19,  
674 3515-3556, <https://doi.org/10.5194/acp-19-3515-2019>, 2019.

675 Jiang, X., Li, G., and Fu, W.: Government environmental governance, structural adjustment and air  
676 quality: A quasi-natural experiment based on the Three-year Action Plan to Win the Blue Sky  
677 Defense War, *Journal of Environmental Management*, 277, 111470,  
678 <https://doi.org/10.1016/j.jenvman.2020.111470>, 2021.

679 Kan, H., Chen, R., and Tong, S.: Ambient air pollution, climate change, and population health in  
680 China, *Environment International*, 42, 10-19, <https://doi.org/10.1016/j.envint.2011.03.003>,  
681 2012.

682 Koukouli, M. E., Theys, N., Ding, J., Zyrichidou, I., Mijling, B., Balis, D., and van der A, R. J.:  
683 Updated SO2 emission estimates over China using OMI/Aura observations, *Atmospheric*  
684 *Measurement Techniques*, 11, 1817-1832, <https://doi.org/10.5194/amt-11-1817-2018>, 2018.

685 Lee, E. J., Kim, M. J., and Lee, J.-S.: Policy Implications of the Clean Heating Transition: A Case  
686 Study of Shanxi, *Energies*, 14, 8431, 2021.

687 Levelt, P. F., Stein Zweers, D. C., Aben, I., Bauwens, M., Borsdorff, T., De Smedt, I., Eskes, H. J.,  
688 Lerot, C., Loyola, D. G., Romahn, F., Stavrou, T., Theys, N., Van Roozendael, M., Veeckind,  
689 J. P., and Verhoelst, T.: Air quality impacts of COVID-19 lockdown measures detected from  
690 space using high spatial resolution observations of multiple trace gases from Sentinel-  
691 5P/TROPOMI, *Atmospheric Chemistry and Physics*, 22, 10319-10351,  
692 <https://doi.org/10.5194/acp-22-10319-2022>, 2022.

693 Li, C., Hammer, M. S., Zheng, B., and Cohen, R. C.: Accelerated reduction of air pollutants in  
694 China, 2017-2020, *Science of The Total Environment*, 803, 150011,  
695 <https://doi.org/10.1016/j.scitotenv.2021.150011>, 2022a.

696 Li, H., Yang, Y., Wang, H., Wang, P., Yue, X., and Liao, H.: Projected Aerosol Changes Driven by  
697 Emissions and Climate Change Using a Machine Learning Method, *Environmental Science &*  
698 *Technology*, 56, 3884-3893, [10.1021/acs.est.1c04380](https://doi.org/10.1021/acs.est.1c04380), 2022b.

699 Li, H., Liang, L., Zhang, S., Qian, Z., Cai, M., Wang, X., McMillin, S. E., Keith, A. E., Wei, J.,



700 Geng, Y., and Lin, H.: Short-term ambient particulate matter pollution of different sizes and  
701 respiratory hospital admission in the Beibu Gulf area of Southern China, *Atmospheric*  
702 *Environment*, 294, 119524, <https://doi.org/10.1016/j.atmosenv.2022.119524>, 2023a.

703 Li, R., Cui, L., Liang, J., Zhao, Y., Zhang, Z., and Fu, H.: Estimating historical SO<sub>2</sub> level across the  
704 whole China during 1973–2014 using random forest model, *Chemosphere*, 247, 125839,  
705 <https://doi.org/10.1016/j.chemosphere.2020.125839>, 2020.

706 Li, R., Wang, Z., Cui, L., Fu, H., Zhang, L., Kong, L., Chen, W., and Chen, J.: Air pollution  
707 characteristics in China during 2015–2016: Spatiotemporal variations and key meteorological  
708 factors, *Science of The Total Environment*, 648, 902-915,  
709 <https://doi.org/10.1016/j.scitotenv.2018.08.181>, 2019.

710 Li, S., Wei, J., Hu, Y., Liu, Y., Hu, M., Shi, Y., Xue, Y., Liu, M., Xie, W., Guo, X., and Liu, X.:  
711 Long-term effect of intermediate particulate matter (PM<sub>1–2.5</sub>) on incident asthma among  
712 middle-aged and elderly adults: A national population-based longitudinal study, *Science of The*  
713 *Total Environment*, 859, 160204, <https://doi.org/10.1016/j.scitotenv.2022.160204>, 2023b.

714 Li, S., Meng, Q., Laba, C., Guan, H., Wang, Z., Pan, Y., Wei, J., Xu, H., Zeng, C., Wang, X., Jiang,  
715 M., Lu, R., Guo, B., and Zhao, X.: Associations between long-term exposure to ambient air  
716 pollution and renal function in Southwest China: The China Multi-Ethnic Cohort (CMEC)  
717 study, *Ecotoxicology and Environmental Safety*, 242, 113851,  
718 <https://doi.org/10.1016/j.ecoenv.2022.113851>, 2022c.

719 Li, T., Shen, H., Yuan, Q., Zhang, X., and Zhang, L.: Estimating Ground-Level PM<sub>2.5</sub> by Fusing  
720 Satellite and Station Observations: A Geo-Intelligent Deep Learning Approach, 44, 11,985-  
721 911,993, <https://doi.org/10.1002/2017GL075710>, 2017b.

722 Li, Y., Yuan, X., Wei, J., Sun, Y., Ni, W., Zhang, H., Zhang, Y., Wang, R., Xu, R., Chen, G., Liu, Y.,  
723 and Xu, J.: Long-term exposure to ambient particulate matter and kidney function in older  
724 adults, *Atmospheric Environment*, 295, 119535,  
725 <https://doi.org/10.1016/j.atmosenv.2022.119535>, 2023c.

726 Li, Y., Yuan, X., Wei, J., Sun, Y., Ni, W., Zhang, H., Zhang, Y., Wang, R., Xu, R., Liu, T., Yang, C.,  
727 Chen, G., Xu, J., and Liu, Y.: Long-term exposure to ambient air pollution and serum liver  
728 enzymes in older adults: A population-based longitudinal study, *Annals of Epidemiology*, 74,  
729 1-7, <https://doi.org/10.1016/j.annepidem.2022.05.011>, 2022d.

730 Li, Z., Guo, J., Ding, A., Liao, H., Liu, J., Sun, Y., Wang, T., Xue, H., Zhang, H., and Zhu, B.:  
731 Aerosol and boundary-layer interactions and impact on air quality, *National Science Review*, 4,  
732 810-833, <https://doi.org/10.1093/nsr/nwx117>, 2017a.

733 Lin, J., Lin, C., Tao, M., Ma, J., Fan, L., Xu, R.-A., and Fang, C.: Spatial Disparity of  
734 Meteorological Impacts on Carbon Monoxide Pollution in China during the COVID-19  
735 Lockdown Period, *ACS Earth and Space Chemistry*, 5, 2900-2909,  
736 <https://doi.org/10.1021/acsearthspacechem.1c00251>, 2021.

737 Ling, C. and Li, Y.: Substantial Changes of Gaseous Pollutants and Health Effects During the  
738 COVID-19 Lockdown Period Across China, *GeoHealth*, 5, e2021GH000408,  
739 <https://doi.org/10.1029/2021GH000408>, 2021.

740 Liu, D., Di, B., Luo, Y., Deng, X., Zhang, H., Yang, F., Grieneisen, M. L., and Zhan, Y.: Estimating  
741 ground-level CO concentrations across China based on the national monitoring network and  
742 MOPITT: potentially overlooked CO hotspots in the Tibetan Plateau, *Atmospheric Chemistry*  
743 *and Physics*, 19, 12413-12430, <https://doi.org/10.5194/acp-19-12413-2019>, 2019.

- 744 Liu, J.: Mapping high resolution national daily NO<sub>2</sub> exposure across mainland China using an  
745 ensemble algorithm, *Environmental Pollution*, 279, 116932,  
746 <https://doi.org/10.1016/j.envpol.2021.116932>, 2021.
- 747 Liu, T., Zhou, Y., Wei, J., Chen, Q., Xu, R., Pan, J., Lu, W., Wang, Y., Fan, Z., Li, Y., Xu, L., Cui, X.,  
748 Shi, C., Zhang, L., Chen, X., Bao, W., Sun, H., and Liu, Y.: Association between short-term  
749 exposure to ambient air pollution and dementia mortality in Chinese adults, *Science of The*  
750 *Total Environment*, 849, 157860, <https://doi.org/10.1016/j.scitotenv.2022.157860>, 2022a.
- 751 Liu, W., Cai, M., Long, Z., Tong, X., Li, Y., Wang, L., Zhou, M., Wei, J., Lin, H., and Yin, P.:  
752 Association between ambient sulfur dioxide pollution and asthma mortality: Evidence from a  
753 nationwide analysis in China, *Ecotoxicology and Environmental Safety*, 249, 114442,  
754 <https://doi.org/10.1016/j.ecoenv.2022.114442>, 2023.
- 755 Liu, W., Wei, J., Cai, M., Qian, Z., Long, Z., Wang, L., Vaughn, M. G., Aaron, H. E., Tong, X., Li,  
756 Y., Yin, P., Lin, H., and Zhou, M.: Particulate matter pollution and asthma mortality in China:  
757 A nationwide time-stratified case-crossover study from 2015 to 2020, *Chemosphere*, 308,  
758 136316, <https://doi.org/10.1016/j.chemosphere.2022.136316>, 2022b.
- 759 Lu, J., Wu, K., Ma, X., Wei, J., Yuan, Z., Huang, Z., Fan, W., Zhong, Q., Huang, Y., and Wu, X.:  
760 Short-term effects of ambient particulate matter (PM<sub>1</sub>, PM<sub>2.5</sub> and PM<sub>10</sub>) on influenza-like  
761 illness in Guangzhou, China, *International Journal of Hygiene and Environmental Health*, 247,  
762 114074, <https://doi.org/10.1016/j.ijheh.2022.114074>, 2023.
- 763 Ma, X., Duan, H., Zhang, H., Liu, X., Sun, X., Wei, J., Zhao, M., and Xi, B.: Short-term effects of  
764 PM<sub>1</sub>, PM<sub>2.5</sub>, and PM<sub>2.5</sub> constituents on myocardial infarction mortality in qingdao, China: A  
765 time-stratified case-crossover analysis, *Atmospheric Environment*, 294, 119478,  
766 <https://doi.org/10.1016/j.atmosenv.2022.119478>, 2023.
- 767 Ma, Z., Dey, S., Christopher, S., Liu, R., Bi, J., Balyan, P., and Liu, Y.: A review of statistical  
768 methods used for developing large-scale and long-term PM<sub>2.5</sub> models from satellite data,  
769 *Remote Sensing of Environment*, 269, 112827, <https://doi.org/10.1016/j.rse.2021.112827>, 2022.
- 770 Maji, K. J. and Sarkar, C.: Spatio-temporal variations and trends of major air pollutants in China  
771 during 2015–2018, *Environmental Science and Pollution Research*, 27, 33792-33808,  
772 <https://doi.org/10.1007/s11356-020-09646-8>, 2020.
- 773 MEE: Technical regulation for selection of ambient air quality monitoring stations (on trial) (in  
774 Chinese), Ministry of Ecology and Environment of the People’s Republic of China, available  
775 at:  
776 <https://www.mee.gov.cn/ywgz/fgbz/bz/bzwb/jcffbz/201309/W020131105548727856307.pdf>,  
777 2013a.
- 778 MEE: Specifications and Test Procedures for Ambient Air Quality Continuous Automated  
779 Monitoring System for SO<sub>2</sub>, NO<sub>2</sub>, O<sub>3</sub> and CO (HJ 654-2013) (in Chinese), Ministry of  
780 Ecology and Environment of the People’s Republic of China, available at:  
781 [https://www.mee.gov.cn/ywgz/fgbz/bz/bzwb/jcffbz/201308/t20130802\\_20256853.shtml](https://www.mee.gov.cn/ywgz/fgbz/bz/bzwb/jcffbz/201308/t20130802_20256853.shtml),  
782 2013b.
- 783 MEE: Technical Specifications for Installation and Acceptance of Ambient Air Quality Continuous  
784 Automated Monitoring System for SO<sub>2</sub>, NO<sub>2</sub>, O<sub>3</sub> and CO (HJ 193-2013) (in Chinese),  
785 Ministry of Ecology and Environment of the People’s Republic of China, 2013c.
- 786 MEE: Revision of the Ambient air quality standards (GB 3095-2012) (in Chinese), Ministry of  
787 Ecology and Environment of the People’s Republic of China, available at:

788 [http://www.mee.gov.cn/xxgk2018/xxgk/xxgk2001/201808/t20180815\\_20629602.html](http://www.mee.gov.cn/xxgk2018/xxgk/xxgk2001/201808/t20180815_20629602.html), 2018a.  
789 MEE: Technical specifications for operation and quality control of ambient air quality continuous  
790 automated monitoring system for SO<sub>2</sub>, NO<sub>2</sub>, O<sub>3</sub> and CO (HJ 818-2018) (in Chinese), Ministry  
791 of Ecology and Environment of the People's Republic of China, available at:  
792 [http://www.cnemc.cn/jcgf/dqhj/202009/t20200922\\_20799646.shtml](http://www.cnemc.cn/jcgf/dqhj/202009/t20200922_20799646.shtml), 2018b.  
793 Mei, Y., Li, A., Zhao, J., Zhou, Q., Zhao, M., Xu, J., Li, R., Li, Y., Li, K., Ge, X., Guo, C., Wei, Y.,  
794 and Xu, Q.: Association of long-term air pollution exposure with the risk of prediabetes and  
795 diabetes: Systematic perspective from inflammatory mechanisms, glucose homeostasis  
796 pathway to preventive strategies, *Environmental Research*, 216, 114472,  
797 <https://doi.org/10.1016/j.envres.2022.114472>, 2023.  
798 Muñoz-Sabater, J., Dutra, E., Agustí-Panareda, A., Albergel, C., Arduini, G., Balsamo, G., Boussetta,  
799 S., Choulga, M., Harrigan, S., Hersbach, H., Martens, B., Miralles, D. G., Piles, M.,  
800 Rodríguez-Fernández, N. J., Zsoter, E., Buontempo, C., and Thépaut, J. N.: ERA5-Land: a  
801 state-of-the-art global reanalysis dataset for land applications, *Earth System Science Data*, 13,  
802 4349-4383, <https://doi.org/10.5194/essd-13-4349-2021>, 2021.  
803 Murray, C. J. L., Aravkin, A. Y., Zheng, P., and al., e.: Global burden of 87 risk factors in 204  
804 countries and territories, 1990&#x2013;2019: a systematic analysis for the Global Burden of  
805 Disease Study 2019, *The Lancet*, 396, 1223-1249, [https://doi.org/10.1016/S0140-](https://doi.org/10.1016/S0140-6736(20)30752-2)  
806 [6736\(20\)30752-2](https://doi.org/10.1016/S0140-6736(20)30752-2), 2020.  
807 Orellano, P., Reynoso, J., Quaranta, N., Bardach, A., and Ciapponi, A.: Short-term exposure to  
808 particulate matter (PM<sub>10</sub> and PM<sub>2.5</sub>), nitrogen dioxide (NO<sub>2</sub>), and ozone (O<sub>3</sub>) and all-cause  
809 and cause-specific mortality: Systematic review and meta-analysis, *Environment International*,  
810 142, 105876, <https://doi.org/10.1016/j.envint.2020.105876>, 2020.  
811 Qin, K., Rao, L., Xu, J., Bai, Y., Zou, J., Hao, N., Li, S., and Yu, C.: Estimating Ground Level NO<sub>2</sub>  
812 Concentrations over Central-Eastern China Using a Satellite-Based Geographically and  
813 Temporally Weighted Regression Model, *Remote Sensing*, 9, 950, 2017.  
814 Rodriguez, J. D., Perez, A., and Lozano, J. A.: Sensitivity Analysis of k-Fold Cross Validation in  
815 Prediction Error Estimation, *IEEE Transactions on Pattern Analysis and Machine Intelligence*,  
816 32, 569-575, <https://doi.org/10.1109/TPAMI.2009.187>, 2010.  
817 Seo, J., Kim, J. Y., Youn, D., Lee, J. Y., Kim, H., Lim, Y. B., Kim, Y., and Jin, H. C.: On the  
818 multiday haze in the Asian continental outflow: the important role of synoptic conditions  
819 combined with regional and local sources, *Atmospheric Chemistry and Physics*, 17, 9311-9332,  
820 <https://doi.org/10.5194/acp-17-9311-2017>, 2017.  
821 Shah, V., Jacob, D. J., Li, K., Silvern, R. F., Zhai, S., Liu, M., Lin, J., and Zhang, Q.: Effect of  
822 changing NO<sub>x</sub> lifetime on the seasonality and long-term trends of satellite-observed  
823 tropospheric NO<sub>2</sub> columns over China, *Atmospheric Chemistry and Physics*, 20, 1483-1495,  
824 <https://doi.org/10.5194/acp-20-1483-2020>, 2020.  
825 Song, J., Du, P., Yi, W., Wei, J., Fang, J., Pan, R., Zhao, F., Zhang, Y., Xu, Z., Sun, Q., Liu, Y., Chen,  
826 C., Cheng, J., Lu, Y., Li, T., Su, H., and Shi, X.: Using an Exposome-Wide Approach to  
827 Explore the Impact of Urban Environments on Blood Pressure among Adults in Beijing–  
828 Tianjin–Hebei and Surrounding Areas of China, *Environmental Science & Technology*,  
829 <https://doi.org/10.1021/acs.est.1c08327>, 2022.  
830 Su, T., Li, Z., Zheng, Y., Luan, Q., and Guo, J.: Abnormally Shallow Boundary Layer Associated  
831 With Severe Air Pollution During the COVID-19 Lockdown in China, *Geophysical Research*

832 Letters, 47, e2020GL090041, <https://doi.org/10.1029/2020GL090041>, 2020.

833 Su, X., Zhang, S., Lin, Q., Wu, Y., Yang, Y., Yu, H., Huang, S., Luo, W., Wang, X., Lin, H., Ma, L.,  
834 and Zhang, Z.: Prenatal exposure to air pollution and neurodevelopmental delay in children: A  
835 birth cohort study in Foshan, China, *Science of The Total Environment*, 816, 151658,  
836 <https://doi.org/10.1016/j.scitotenv.2021.151658>, 2022.

837 Tian, H., Liu, Y., Li, Y., Wu, C.-H., Chen, B., Kraemer, M. U. G., Li, B., Cai, J., Xu, B., Yang, Q.,  
838 Wang, B., Yang, P., Cui, Y., Song, Y., Zheng, P., Wang, Q., Bjornstad, O. N., Yang, R., Grenfell,  
839 B. T., Pybus, O. G., and Dye, C.: An investigation of transmission control measures during the  
840 first 50 days of the COVID-19 epidemic in China, *Science*, 368, 638-642,  
841 <https://doi.org/10.1126/science.abb6105>, 2020.

842 van der A, R. J., Mijling, B., Ding, J., Koukouli, M. E., Liu, F., Li, Q., Mao, H., and Theys, N.:  
843 Cleaning up the air: effectiveness of air quality policy for SO<sub>2</sub> and NO<sub>x</sub> emissions in China,  
844 *Atmospheric Chemistry and Physics*, 17, 1775-1789, [https://doi.org/10.5194/acp-17-1775-](https://doi.org/10.5194/acp-17-1775-2017)  
845 2017, 2017.

846 Wan, J., Qin, C., Wang, Q., Xiao, Y., Niu, R., Li, X., and Su, J.: A Brief Overview of the 13th Five-  
847 Year Plan for the Protection of Ecological Environment, in: *Environmental Strategy and*  
848 *Planning in China*, edited by: Wang, J., Wang, X., and Wan, J., Springer Singapore, Singapore,  
849 57-85, [https://doi.org/10.1007/978-981-16-6909-5\\_3](https://doi.org/10.1007/978-981-16-6909-5_3), 2022.

850 Wang, L., Zhang, J., Wei, J., Zong, J., Lu, C., Du, Y., and Wang, Q.: Association of ambient air  
851 pollution exposure and its variability with subjective sleep quality in China: A multilevel  
852 modeling analysis, *Environmental Pollution*, 312, 120020,  
853 <https://doi.org/10.1016/j.envpol.2022.120020>, 2022a.

854 Wang, R., Xu, R., Wei, J., Liu, T., Ye, Y., Li, Y., Lin, Q., Zhou, Y., Huang, S., Lv, Z., Tian, Q., and  
855 Liu, Y.: Short-Term Exposure to Ambient Air Pollution and Hospital Admissions for Sequelae  
856 of Stroke in Chinese Older Adults, *GeoHealth*, 6, e2022GH000700,  
857 <https://doi.org/10.1029/2022GH000700>, 2022b.

858 Wang, S., Su, H., Chen, C., Tao, W., Streets, D. G., Lu, Z., Zheng, B., Carmichael, G. R., Lelieveld,  
859 J., Pöschl, U., and Cheng, Y.: Natural gas shortages during the "coal-to-gas" transition in China  
860 have caused a large redistribution of air pollution in winter 2017, *Proceedings of the National*  
861 *Academy of Sciences*, 117, 31018-31025, <https://doi.org/10.1073/pnas.2007513117>, 2020a.

862 Wang, Y., Yuan, Q., Li, T., Zhu, L., and Zhang, L.: Estimating daily full-coverage near surface O<sub>3</sub>,  
863 CO, and NO<sub>2</sub> concentrations at a high spatial resolution over China based on S5P-TROPOMI  
864 and GEOS-FP, *ISPRS Journal of Photogrammetry and Remote Sensing*, 175, 311-325,  
865 <https://doi.org/10.1016/j.isprsjprs.2021.03.018>, 2021.

866 Wang, Y., Ma, Y. F., Eskes, H., Inness, A., Flemming, J., and Brasseur, G. P.: Evaluation of the  
867 CAMS global atmospheric trace gas reanalysis 2003–2016 using aircraft campaign  
868 observations, *Atmospheric Chemistry and Physics*, 20, 4493-4521, [https://doi.org/10.5194/acp-](https://doi.org/10.5194/acp-20-4493-2020)  
869 20-4493-2020, 2020b.

870 Wang, Y., Luo, S., Wei, J., Yang, Z., Hu, K., Yao, Y., and Zhang, Y.: Ambient NO<sub>2</sub> exposure hinders  
871 long-term survival of Chinese middle-aged and older adults, *Science of The Total Environment*,  
872 855, 158784, <https://doi.org/10.1016/j.scitotenv.2022.158784>, 2023.

873 Wei, J., Li, Z., Guo, J., Sun, L., Huang, W., Xue, W., Fan, T., and Cribb, M.: Satellite-Derived 1-  
874 km-Resolution PM<sub>1</sub> Concentrations from 2014 to 2018 across China, *Environmental Science*  
875 *& Technology*, 53, 13265-13274, <https://doi.org/10.1021/acs.est.9b03258>, 2019.

- 876 Wei, J., Li, Z., Lyapustin, A., Sun, L., Peng, Y., Xue, W., Su, T., and Cribb, M.: Reconstructing 1-  
877 km-resolution high-quality PM<sub>2.5</sub> data records from 2000 to 2018 in China: spatiotemporal  
878 variations and policy implications, *Remote Sensing of Environment*, 252, 112136,  
879 <https://doi.org/10.1016/j.rse.2020.112136>, 2021a.
- 880 Wei, J., Li, Z., Xue, W., Sun, L., Fan, T., Liu, L., Su, T., and Cribb, M.: The ChinaHighPM10  
881 dataset: generation, validation, and spatiotemporal variations from 2015 to 2019 across China,  
882 *Environment International*, 146, 106290, <https://doi.org/10.1016/j.envint.2020.106290>, 2021b.
- 883 Wei, J., Li, Z., Li, K., Dickerson, R. R., Pinker, R. T., Wang, J., Liu, X., Sun, L., Xue, W., and Cribb,  
884 M.: Full-coverage mapping and spatiotemporal variations of ground-level ozone (O<sub>3</sub>) pollution  
885 from 2013 to 2020 across China, *Remote Sensing of Environment*, 270, 112775,  
886 <https://doi.org/10.1016/j.rse.2021.112775>, 2022a.
- 887 Wei, J., Li, Z., Cribb, M., Huang, W., Xue, W., Sun, L., Guo, J., Peng, Y., Li, J., Lyapustin, A., Liu,  
888 L., Wu, H., and Song, Y.: Improved 1&thinsp;km resolution PM<sub>2.5</sub> estimates across China  
889 using enhanced space–time extremely randomized trees, *Atmospheric Chemistry and Physics*,  
890 20, 3273-3289, <https://doi.org/10.5194/acp-20-3273-2020>, 2020.
- 891 Wei, J., Liu, S., Li, Z., Liu, C., Qin, K., Liu, X., Pinker, R. T., Dickerson, R. R., Lin, J., Boersma, K.  
892 F., Sun, L., Li, R., Xue, W., Cui, Y., Zhang, C., and Wang, J.: Ground-Level NO<sub>2</sub> Surveillance  
893 from Space Across China for High Resolution Using Interpretable Spatiotemporally Weighted  
894 Artificial Intelligence, *Environmental Science & Technology*,  
895 <https://doi.org/10.1021/acs.est.2c03834>, 2022b.
- 896 WHO: Coronavirus Disease (COVID-19) Pandemic, The World Health Organization, Available  
897 online: [https://www.who.int/  
898 WHO: WHO global air quality guidelines. Particulate matter \(PM<sub>2.5</sub> and PM<sub>10</sub>\), ozone, nitrogen  
899 dioxide, sulfur dioxide and carbon monoxide, Geneva: World Health Organization, Licence:  
900 CC BY-NC-SA 3.0 IGO, Licence: CC BY-NC-SA 3.0 IGO, 2021.](https://www.who.int/emergencies/diseases/novel-coronavirus-2019)
- 901 Wu, H., Zhang, Y., Zhao, M., Liu, W., Magnussen, C. G., Wei, J., and Xi, B.: Short-term effects of  
902 exposure to ambient PM<sub>1</sub> on blood pressure in children and adolescents aged 9 to 18 years in  
903 Shandong Province, China, *Atmospheric Environment*, 283, 119180,  
904 <https://doi.org/10.1016/j.atmosenv.2022.119180>, 2022a.
- 905 Wu, H., Lu, Z., Wei, J., Zhang, B., Liu, X., Zhao, M., Liu, W., Guo, X., and Xi, B.: Effects of the  
906 COVID-19 Lockdown on Air Pollutant Levels and Associated Reductions in Ischemic Stroke  
907 Incidence in Shandong Province, China, *Frontiers in Public Health*, 10,  
908 <https://doi.org/10.3389/fpubh.2022.876615>, 2022b.
- 909 Wu, S., Huang, B., Wang, J., He, L., Wang, Z., Yan, Z., Lao, X., Zhang, F., Liu, R., and Du, Z.:  
910 Spatiotemporal mapping and assessment of daily ground NO<sub>2</sub> concentrations in China using  
911 high-resolution TROPOMI retrievals, *Environmental Pollution*, 273, 116456,  
912 <https://doi.org/10.1016/j.envpol.2021.116456>, 2021.
- 913 Wu, X., Yang, Y., Gong, Y., Deng, Z., Wang, Y., Wu, W., Zheng, C., and Zhang, Y.: Advances in air  
914 pollution control for key industries in China during the 13th five-year plan, *Journal of  
915 Environmental Sciences*, <https://doi.org/10.1016/j.jes.2022.09.008>, 2022c.
- 916 Xu, H., Bechle, M. J., Wang, M., Szpiro, A. A., Vedal, S., Bai, Y., and Marshall, J. D.: National  
917 PM<sub>2.5</sub> and NO<sub>2</sub> exposure models for China based on land use regression, satellite  
918 measurements, and universal kriging, *Science of The Total Environment*, 655, 423-433,  
919 <https://doi.org/10.1016/j.scitotenv.2018.11.125>, 2019.

- 920 Xu, J., Zhou, J., Luo, P., Mao, D., Xu, W., Nima, Q., Cui, C., Yang, S., Ao, L., Wu, J., Wei, J., Chen,  
921 G., Li, S., Guo, Y., Zhang, J., Liu, Z., and Zhao, X.: Associations of long-term exposure to  
922 ambient air pollution and physical activity with insomnia in Chinese adults, *Science of The*  
923 *Total Environment*, 792, 148197, <https://doi.org/10.1016/j.scitotenv.2021.148197>, 2021.
- 924 Xu, R., Wei, J., Liu, T., Li, Y., Yang, C., Shi, C., Chen, G., Zhou, Y., Sun, H., and Liu, Y.:  
925 Association of short-term exposure to ambient PM1 with total and cause-specific  
926 cardiovascular disease mortality, *Environment International*, 169, 107519,  
927 <https://doi.org/10.1016/j.envint.2022.107519>, 2022a.
- 928 Xu, R., Shi, C., Wei, J., Lu, W., Li, Y., Liu, T., Wang, Y., Zhou, Y., Chen, G., Sun, H., and Liu, Y.:  
929 Cause-specific cardiovascular disease mortality attributable to ambient temperature: A time-  
930 stratified case-crossover study in Jiangsu province, China, *Ecotoxicology and Environmental*  
931 *Safety*, 236, 113498, <https://doi.org/10.1016/j.ecoenv.2022.113498>, 2022b.
- 932 Xu, R., Wang, Q., Wei, J., Lu, W., Wang, R., Liu, T., Wang, Y., Fan, Z., Li, Y., Xu, L., Shi, C., Li, G.,  
933 Chen, G., Zhang, L., Zhou, Y., Liu, Y., and Sun, H.: Association of short-term exposure to  
934 ambient air pollution with mortality from ischemic and hemorrhagic stroke, *European Journal*  
935 *of Neurology*, 29, 1994-2005, <https://doi.org/10.1111/ene.15343>, 2022c.
- 936 Xu, W. Y., Zhao, C. S., Ran, L., Deng, Z. Z., Liu, P. F., Ma, N., Lin, W. L., Xu, X. B., Yan, P., He,  
937 X., Yu, J., Liang, W. D., and Chen, L. L.: Characteristics of pollutants and their correlation to  
938 meteorological conditions at a suburban site in the North China Plain, *Atmos. Chem. Phys.*, 11,  
939 4353-4369, <https://doi.org/10.5194/acp-11-4353-2011>, 2011.
- 940 Yang, Y., Ren, L., Wu, M., Wang, H., Song, F., Leung, L. R., Hao, X., Li, J., Chen, L., Li, H., Zeng,  
941 L., Zhou, Y., Wang, P., Liao, H., Wang, J., and Zhou, Z.-Q.: Abrupt emissions reductions  
942 during COVID-19 contributed to record summer rainfall in China, *Nature Communications*, 13,  
943 959, <https://doi.org/10.1038/s41467-022-28537-9>, 2022.
- 944 Yoo, J.-M., Lee, Y.-R., Kim, D., Jeong, M.-J., Stockwell, W. R., Kundu, P. K., Oh, S.-M., Shin, D.-  
945 B., and Lee, S.-J.: New indices for wet scavenging of air pollutants (O<sub>3</sub>, CO, NO<sub>2</sub>, SO<sub>2</sub>, and  
946 PM<sub>10</sub>) by summertime rain, *Atmospheric Environment*, 82, 226-237,  
947 <https://doi.org/10.1016/j.atmosenv.2013.10.022>, 2014.
- 948 Zhan, Y., Luo, Y., Deng, X., Zhang, K., Zhang, M., Grieneisen, M. L., and Di, B.: Satellite-Based  
949 Estimates of Daily NO<sub>2</sub> Exposure in China Using Hybrid Random Forest and Spatiotemporal  
950 Kriging Model, *Environmental Science & Technology*, 52, 4180-4189,  
951 10.1021/acs.est.7b05669, 2018.
- 952 Zhang, B., Rong, Y., Yong, R., Qin, D., Li, M., Zou, G., and Pan, J.: Deep learning for air pollutant  
953 concentration prediction: A review, *Atmospheric Environment*, 290, 119347,  
954 <https://doi.org/10.1016/j.atmosenv.2022.119347>, 2022a.
- 955 Zhang, C., Liu, C., Hu, Q., Cai, Z., Su, W., Xia, C., Zhu, Y., Wang, S., and Liu, J.: Satellite UV-Vis  
956 spectroscopy: implications for air quality trends and their driving forces in China during 2005–  
957 2017, *Light: Science & Applications*, 8, 100, <https://doi.org/10.1038/s41377-019-0210-6>,  
958 2019a.
- 959 Zhang, Q., Zheng, Y., Tong, D., Shao, M., Wang, S., Zhang, Y., Xu, X., Wang, J., He, H., Liu, W.,  
960 Ding, Y., Lei, Y., Li, J., Wang, Z., Zhang, X., Wang, Y., Cheng, J., Liu, Y., Shi, Q., Yan, L.,  
961 Geng, G., Hong, C., Li, M., Liu, F., Zheng, B., Cao, J., Ding, A., Gao, J., Fu, Q., Huo, J., Liu,  
962 B., Liu, Z., Yang, F., He, K., and Hao, J.: Drivers of improved PM<sub>2.5</sub> air quality in China from  
963 2013 to 2017, 116, 24463-24469, <https://doi.org/10.1073/pnas.1907956116>, 2019b.

964 Zhang, Y., Li, Z., Wei, J., Zhan, Y., Liu, L., Yang, Z., Zhang, Y., Liu, R., and Ma, Z.: Long-term  
965 exposure to ambient NO<sub>2</sub> and adult mortality: A nationwide cohort study in China, *Journal of*  
966 *Advanced Research*, 41, 13-22, <https://doi.org/10.1016/j.jare.2022.02.007>, 2022b.

967 Zhang, Z., Wang, J., Hart, J. E., Laden, F., Zhao, C., Li, T., Zheng, P., Li, D., Ye, Z., and Chen, K.:  
968 National scale spatiotemporal land-use regression model for PM<sub>2.5</sub>, PM<sub>10</sub> and NO<sub>2</sub>  
969 concentration in China, *Atmospheric Environment*, 192, 48-54,  
970 <https://doi.org/10.1016/j.atmosenv.2018.08.046>, 2018.

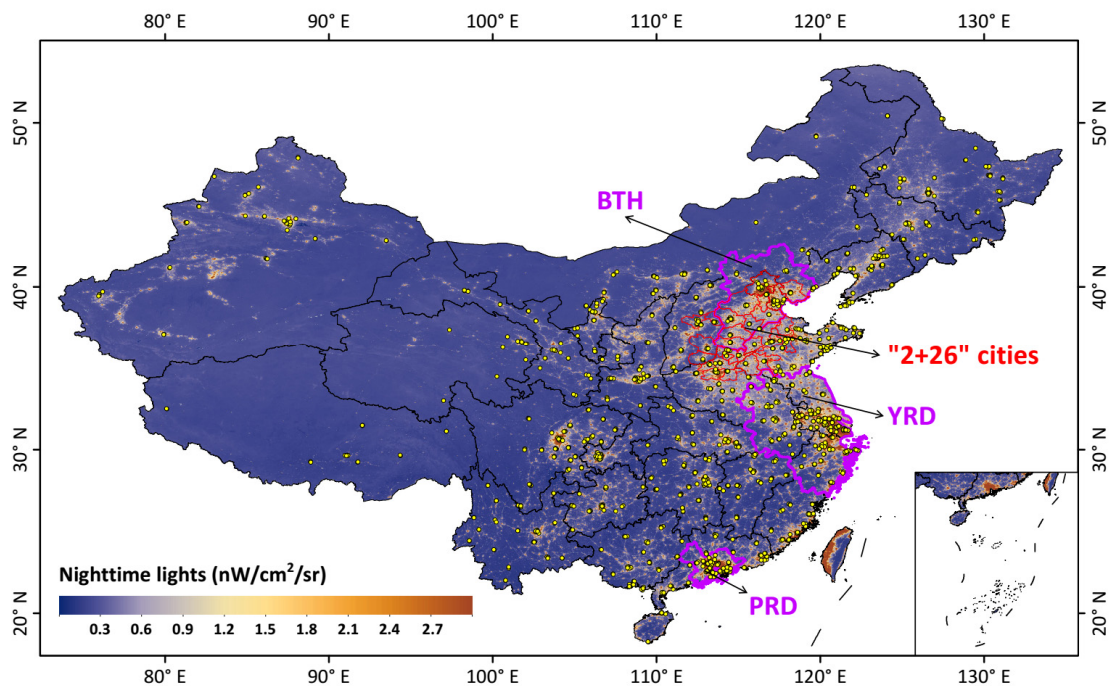
971 Zheng, B., Zhang, Q., Geng, G., Chen, C., Shi, Q., Cui, M., Lei, Y., and He, K.: Changes in China's  
972 anthropogenic emissions and air quality during the COVID-19 pandemic in 2020, *Earth*  
973 *System Science Data*, 13, 2895-2907, <https://doi.org/10.5194/essd-13-2895-2021>, 2021.

974 Zheng, B., Chevallier, F., Ciais, P., Yin, Y., Deeter, M. N., Worden, H. M., Wang, Y., Zhang, Q., and  
975 He, K.: Rapid decline in carbon monoxide emissions and export from East Asia between years  
976 2005 and 2016, *Environmental Research Letters*, 13, 044007, [https://doi.org/10.1088/1748-](https://doi.org/10.1088/1748-9326/aab2b3)  
977 [9326/aab2b3](https://doi.org/10.1088/1748-9326/aab2b3), 2018.

978

979 **Figures**

980



981

982

983

984

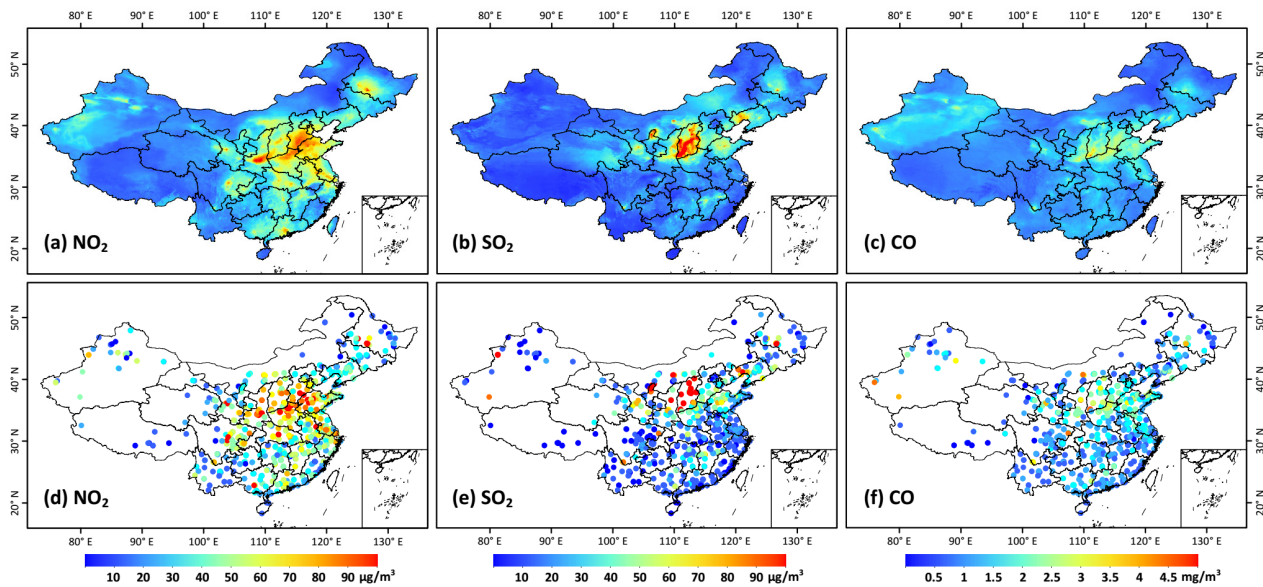
985

986

987

**Figure 1.** Geographical locations of ground-based stations from the China National Environmental Monitoring Centre network (marked as yellow dots) monitoring gaseous pollutants across China. The background shows the nighttime-light level, an estimate of population. Purple boundaries three typical urban agglomerations: the Beijing-Tianjin-Hebei (BTH) region, the Yangtze River Delta (YRD), and the Pearl River Delta (PRD).





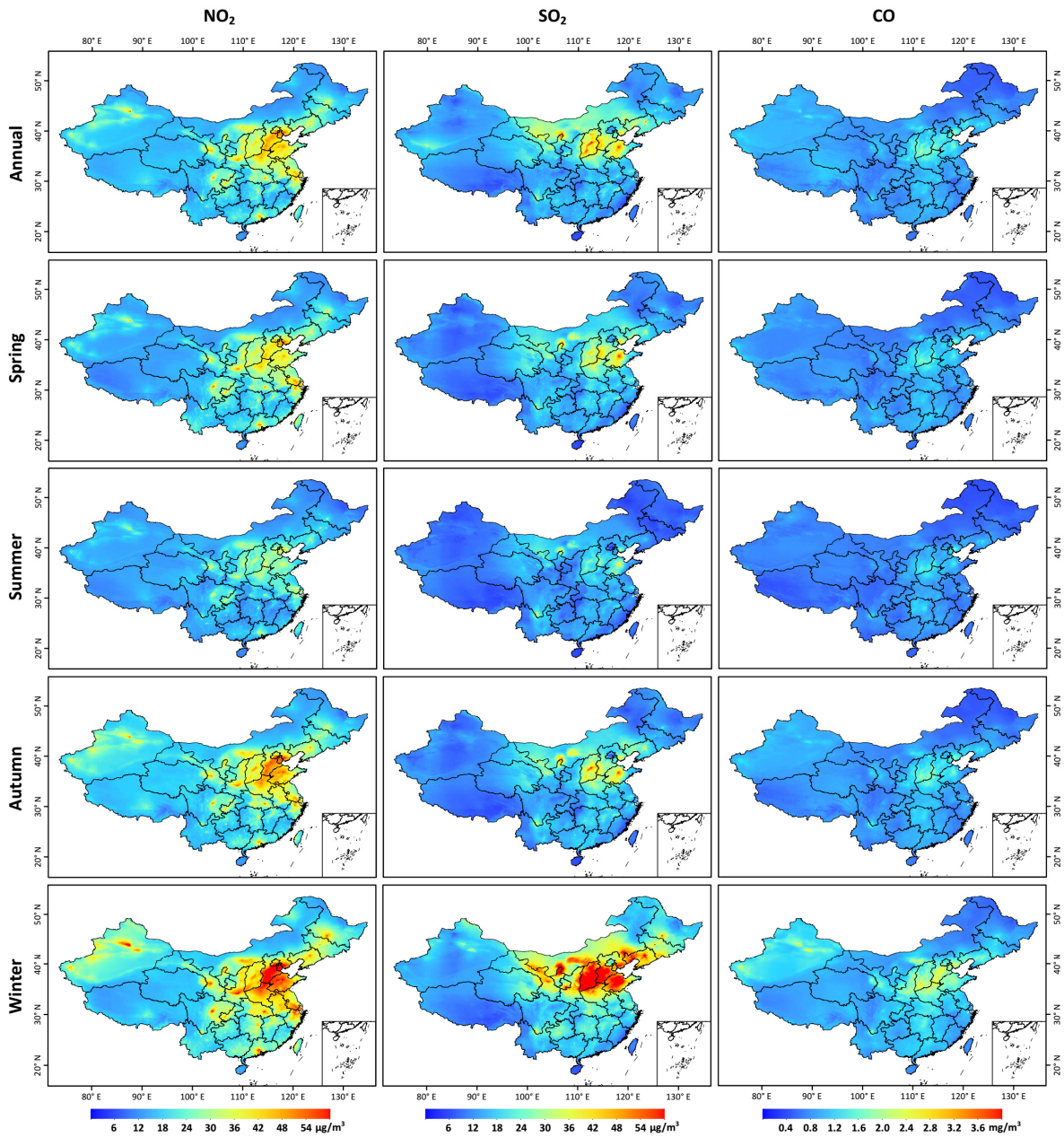
988

989

990

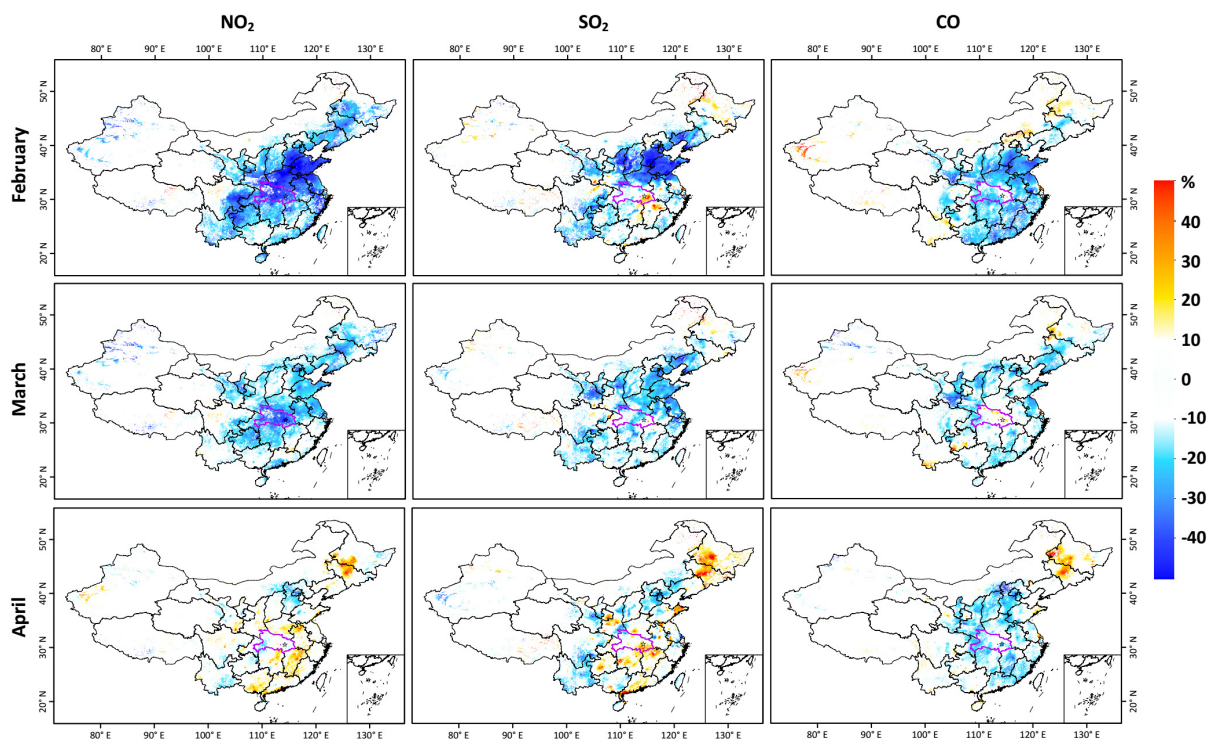
991

**Figure 2.** A typical example of (a-c) big-data-derived (horizontal resolution = 10 km) seamless surface NO<sub>2</sub> (µg/m<sup>3</sup>), SO<sub>2</sub> (µg/m<sup>3</sup>), and CO (mg/m<sup>3</sup>) concentrations and (d-f) corresponding ground measurements on 1 January 2018 in China.



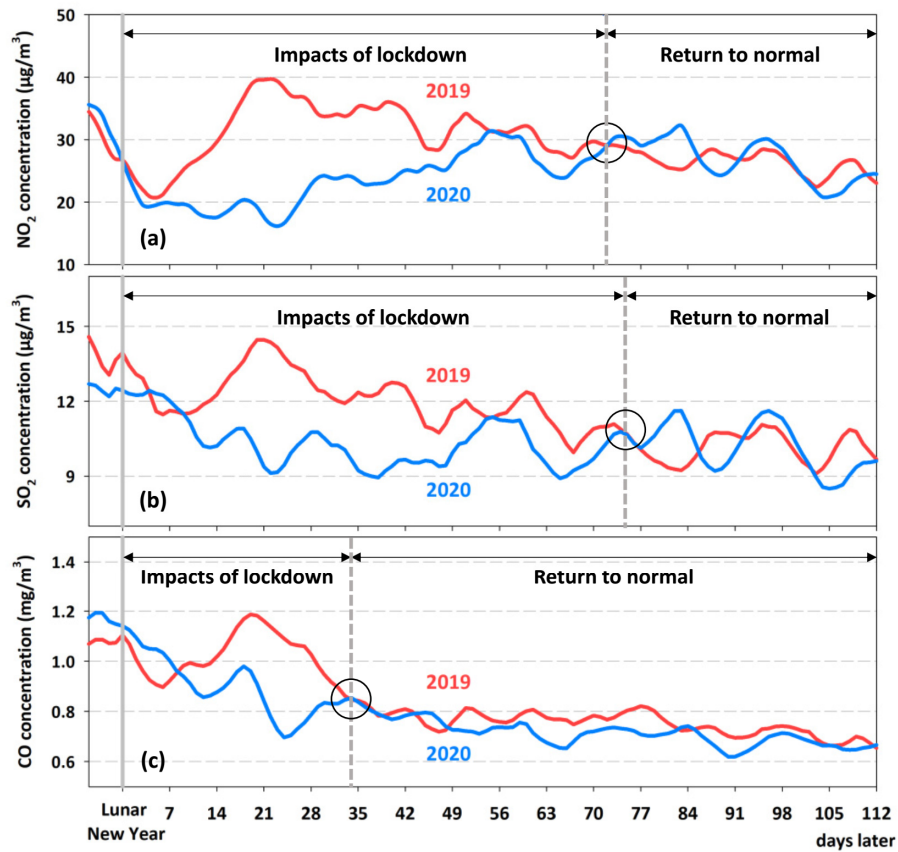
992  
993  
994

**Figure 3.** Annual and seasonal mean maps (horizontal resolution = 10 km) of surface NO<sub>2</sub> (µg/m<sup>3</sup>), SO<sub>2</sub> (µg/m<sup>3</sup>), and CO (mg/m<sup>3</sup>) averaged over the period 2013–2020 in China.



995  
 996  
 997  
 998  
 999

**Figure 4.** Relative changes (%) in surface  $\text{NO}_2$ ,  $\text{SO}_2$ , and  $\text{CO}$  concentrations in February, March, and April between 2019 and 2020 in populated areas of China. The area outlined in magenta and the star in each panel indicate Hubei Province and Wuhan City, respectively.



1000  
 1001  
 1002  
 1003  
 1004  
 1005

**Figure 5.** Time series of the seven-day moving averages of daily population-weighted surface (a) NO<sub>2</sub>, (b) SO<sub>2</sub>, and (c) CO concentrations after the Lunar New Year of 2019 and 2020 in China. The black circle in each panel shows the turning point when the gaseous pollutants began to return to their normal levels.

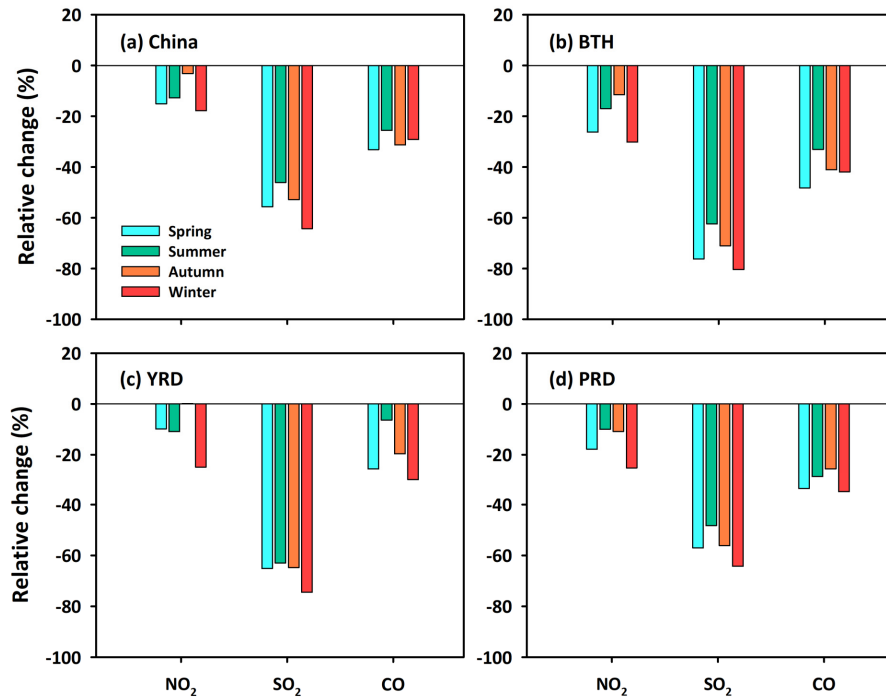


**Figure 6.** Relative changes (%) in seasonal mean surface NO<sub>2</sub>, SO<sub>2</sub>, and CO concentrations between 2013 and 2020 over (a) China, (b) the Beijing-Tianjin-Hebei (BTH) region, (c) the Yangtze River Delta (YRD), and (d) the Pearl River Delta (PRD).

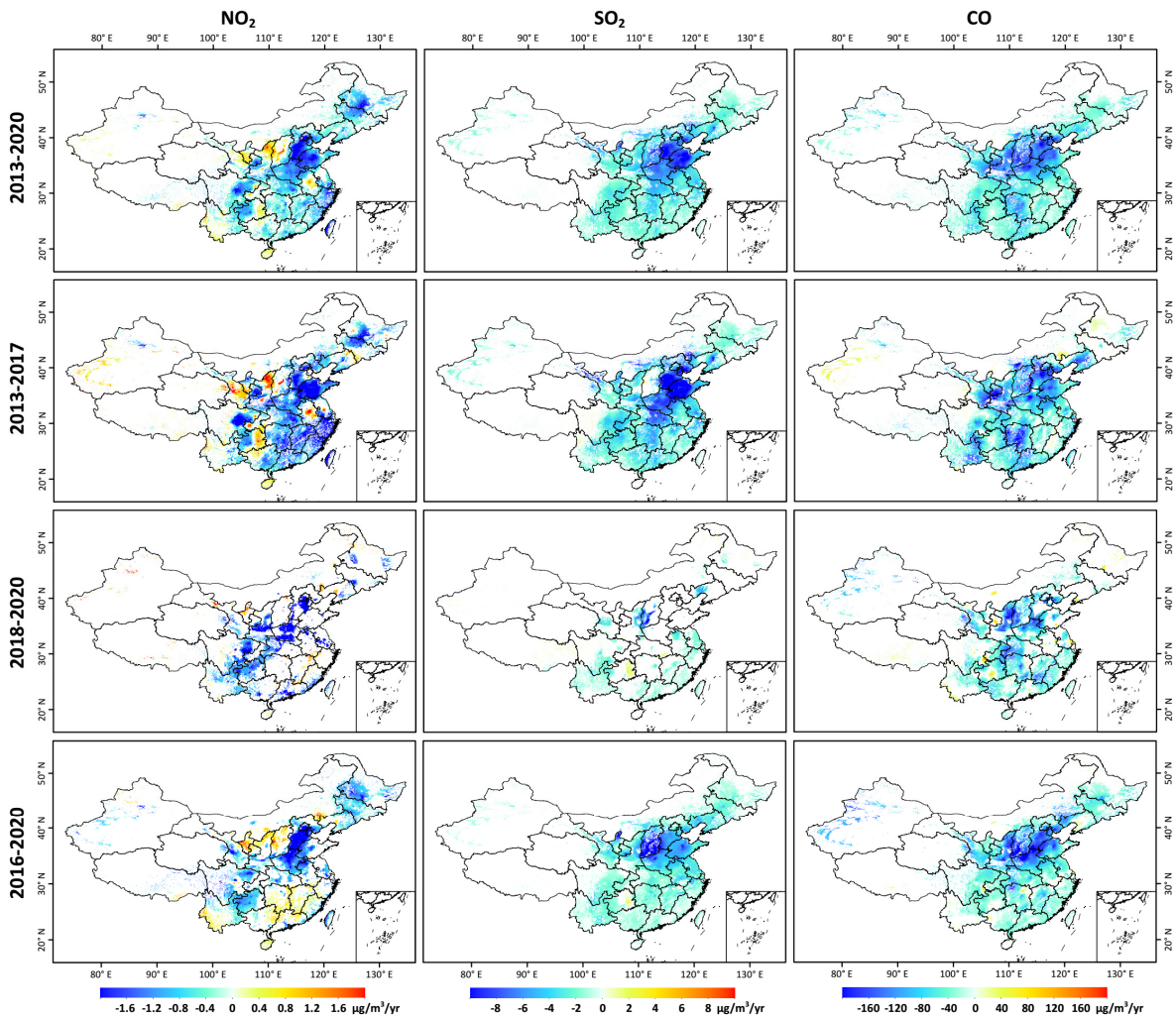
1006

1007

1008

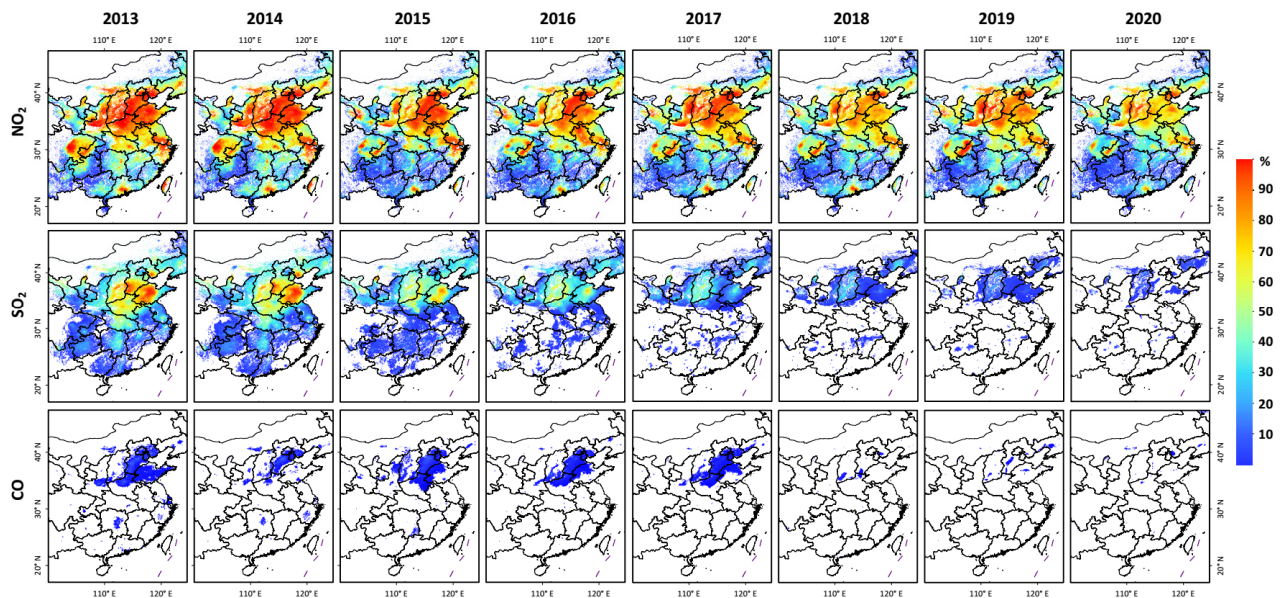
1009

1010



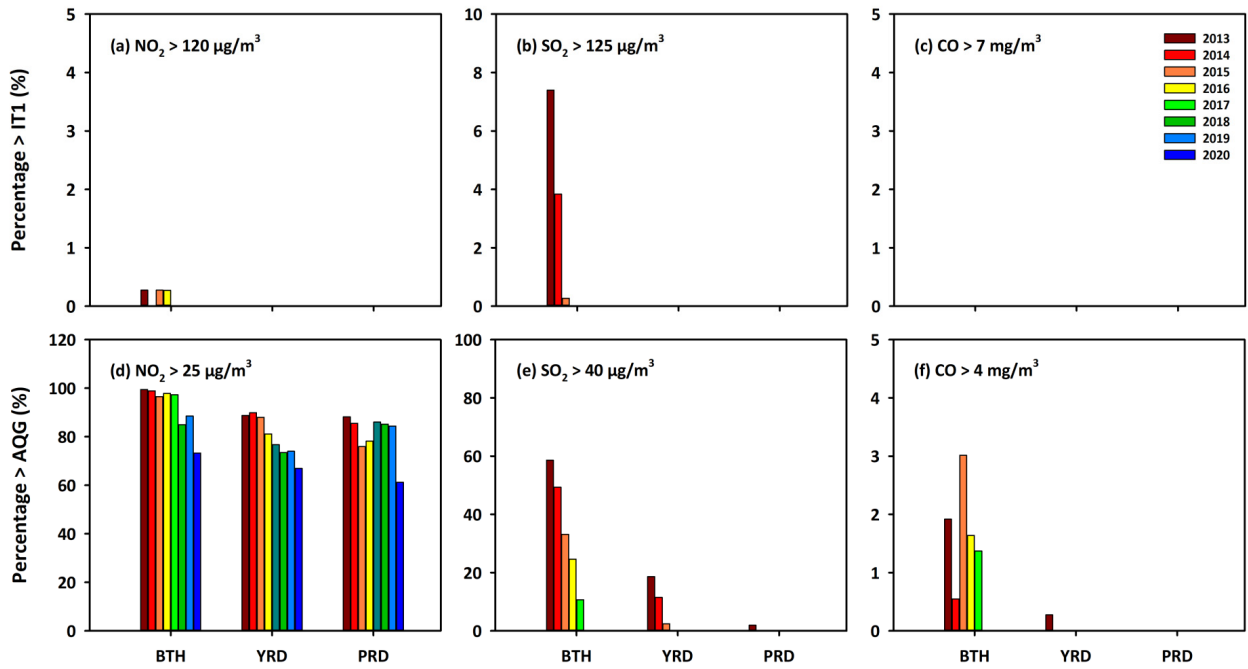
1011  
 1012  
 1013  
 1014  
 1015  
 1016

**Figure 7.** Temporal trends of surface NO<sub>2</sub>, SO<sub>2</sub>, and CO concentrations during the whole period (2013–2020), the Clean Air Action Plan (2013–2017), the Blue Sky Defense War (2018–2020), and the 13rd Five-Year Plan (2016–2020) in populated areas of China. Only regions with trends that are significant at the 95% ( $p < 0.05$ ) confidence level are shown.



1017  
 1018  
 1019  
 1020  
 1021  
 1022

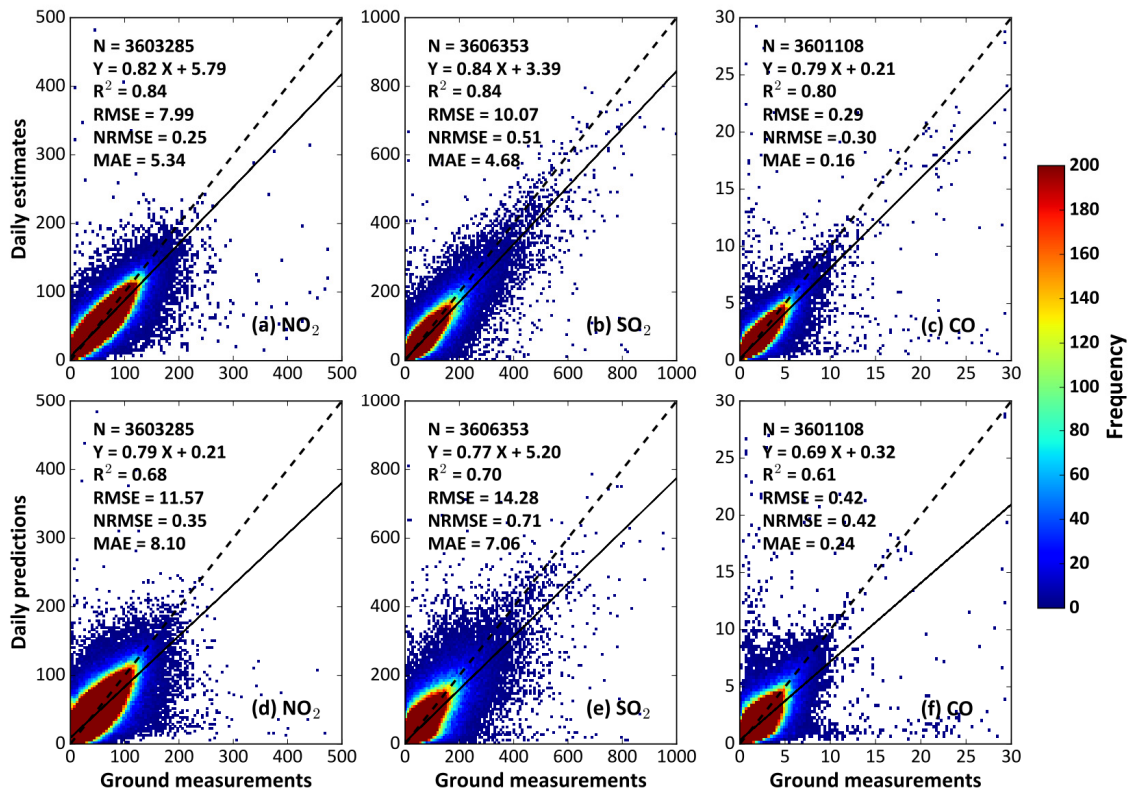
**Figure 8.** Spatial distributions of the percentage of days exceeding the WHO recommended short-term desired air quality guidelines (AQG) level for surface NO<sub>2</sub> (daily mean > 25 μg/m<sup>3</sup>), SO<sub>2</sub> (daily mean > 40 μg/m<sup>3</sup>), and CO (daily mean > 4 mg/m<sup>3</sup>) for each year from 2013 to 2020 in populated areas of eastern China.



1023  
 1024  
 1025  
 1026  
 1027  
 1028

**Figure 9.** Percentage of days (%) exceeding the WHO recommended short-term (a-c) minimum interim target (IT1) and (d-f) desired air quality guidelines (AQG) level for surface NO<sub>2</sub>, SO<sub>2</sub>, and CO for each year from 2013 to 2020 in three typical urban agglomerations: the Beijing-Tianjin-Hebei (BTH) region, the Yangtze River Delta (YRD), and the Pearl River Delta (PRD).





1029

1030

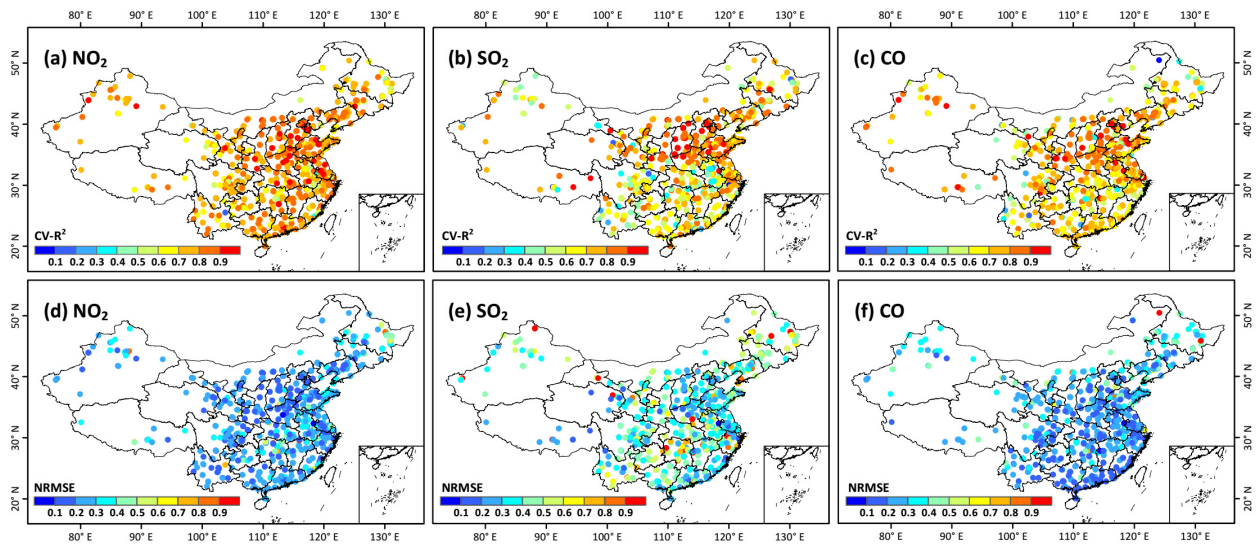
1031

1032

1033

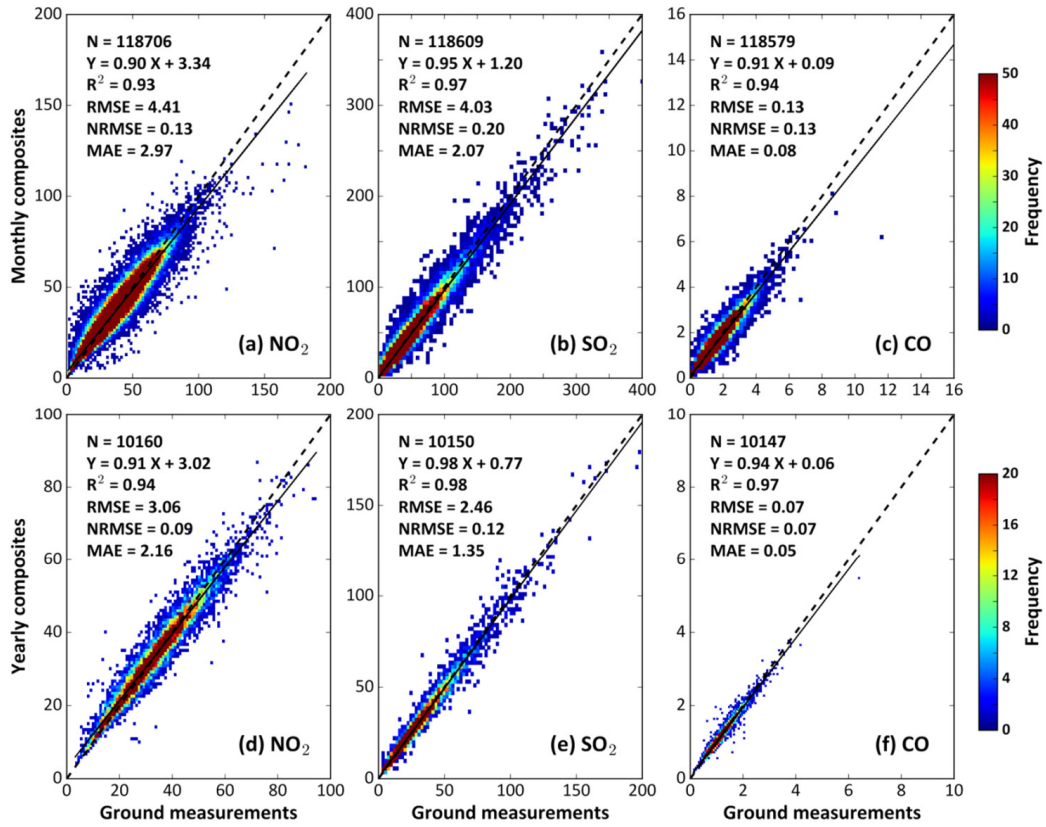
1034

**Figure 10.** Density plots of daily (a-c) estimates and (d-f) predictions of ground-level  $\text{NO}_2$  ( $\mu\text{g}/\text{m}^3$ ),  $\text{SO}_2$  ( $\mu\text{g}/\text{m}^3$ ), and  $\text{CO}$  ( $\text{mg}/\text{m}^3$ ) concentrations as a function of ground measurements in China from 2013 to 2020 using the out-of-sample (top panels) and out-of-station (bottom panels) cross-validation methods.



1035  
 1036  
 1037  
 1038  
 1039

**Figure 11.** Sample-based spatial validation of daily ground-level NO<sub>2</sub> ( $\mu\text{g}/\text{m}^3$ ), SO<sub>2</sub> ( $\mu\text{g}/\text{m}^3$ ), and CO ( $\text{mg}/\text{m}^3$ ) estimates at each individual monitoring station in China from 2013 to 2020: (a-c) accuracy (i.e., CV-R<sup>2</sup>) and (d-f) uncertainty (i.e., NRMSE).



1040

1041

1042

1043

1044

**Figure 12.** Sample-based temporal validation of (a-c) monthly and (d-f) yearly composites of ground-level  $\text{NO}_2$  ( $\mu\text{g}/\text{m}^3$ ),  $\text{SO}_2$  ( $\mu\text{g}/\text{m}^3$ ), and  $\text{CO}$  ( $\text{mg}/\text{m}^3$ ) as a function of ground measurements from 2013 to 2020 in China.

1045 **Tables**

1046

1047 **Table 1.** Statistics of the overall accuracies and predictive abilities of ambient gaseous pollutants for  
1048 each year in China from 2013 to 2020.

Year	Sample size N (10 <sup>3</sup> )	Overall accuracy						Predictive ability					
		NO <sub>2</sub>		SO <sub>2</sub>		CO		NO <sub>2</sub>		SO <sub>2</sub>		CO	
		R <sup>2</sup>	RMSE	R <sup>2</sup>	RMSE	R <sup>2</sup>	RMSE	R <sup>2</sup>	RMSE	R <sup>2</sup>	RMSE	R <sup>2</sup>	RMSE
2013	169	0.77	12.48	0.83	17.97	0.80	0.56	0.53	18.16	0.68	25.04	0.60	0.78
2014	324	0.76	10.97	0.83	15.87	0.77	0.38	0.54	15.56	0.66	22.45	0.51	0.57
2015	518	0.79	9.34	0.80	13.71	0.74	0.38	0.61	13.10	0.61	19.49	0.50	0.55
2016	516	0.82	8.59	0.83	11.26	0.76	0.34	0.64	12.20	0.65	16.28	0.57	0.46
2017	527	0.86	7.57	0.86	7.79	0.82	0.24	0.72	10.67	0.74	10.80	0.70	0.32
2018	513	0.87	6.92	0.83	5.61	0.82	0.20	0.76	9.33	0.68	7.80	0.69	0.26
2019	515	0.87	6.78	0.81	4.84	0.82	0.20	0.77	9.23	0.66	6.63	0.70	0.25
2020	522	0.89	5.78	0.80	4.02	0.82	0.17	0.79	8.04	0.62	5.57	0.69	0.23

1049

1050

**Table 2.** Comparison of long-term datasets of different gaseous pollutants in China.

Species	Model	Missing values	Spatial resolution	Main input	Validation period	CV-R <sup>2</sup>	RMSE	Literature
NO <sub>2</sub>	RF-STK	Yes	0.25°	OMI	2013–2016	0.62	13.3	(Zhan et al., 2018)
	RF-K	Yes	0.25°	OMI	2013–2018	0.64	11.4	(Dou et al., 2021)
	KCS	Yes	0.125°	OMI	2014–2016	0.72	7.9	(Chen et al., 2019)
	LUR	Yes	0.125°	OMI	2014–2015	0.78	-	(Xu et al., 2019)
	LME	Yes	0.1°	OMI	2014–2020	0.65	7.9	(Chi et al., 2021)
	XGBoost	Yes	0.125°	TROPOMI	2018–2020	0.67	6.4	(Chi et al., 2022)
	XGBoost	Yes	0.05°	TROPOMI	2018–2019	0.83	7.6	(Liu, 2021)
	LightGBM	No	0.05°	TROPOMI	2018–2020	0.83	6.6	(Wang et al., 2021)
	SWDF	No	0.01°	TROPOMI	2019–2020	0.93	4.9	(Wei et al., 2022b)
STET	No	0.1°	Big data	2013–2020	0.84	8.0	This study	
SO <sub>2</sub>	RF	No	0.25°	Emissions	2013–2014	0.64	17.1	(Li et al., 2020)
	STET	No	0.1	Big data	2013–2020	0.84	10.1	This study
CO	RF-STK	Yes	0.1	MOPITT	2013–2016	0.51	0.54	(Liu et al., 2019)
	LightGBM	No	0.07°	TROPOMI	2018–2020	0.71	0.26	(Wang et al., 2021)
	STET	No	0.1°	Big data	2013–2020	0.80	0.29	This study

1051

KCS: kriging-calibrated satellite method; LightGBM: light gradient boosted model; LME: linear mixed effect model;

1052

LUR: land use regression; MOPITT: Measurements of Pollution in the Troposphere; OMI: Ozone Monitoring

1053

Instrument; RF: random forest; RF-K: random forest integrated with K-means; RF-STK: random-forest-spatiotemporal-

1054

kriging model; STET: space-time extremely randomized tree; SWDF: spatiotemporally weighted deep forest;

1055

TROPOMI: TROPospheric Monitoring Instrument; XGBoost: extreme gradient boosting